### Title
Trace gas mixing ratio variability versus lifetime in the troposphere and stratosphere: Observations




### Journal
Journal of Geophysical Research, 104(D13)

### ISSN
0148-0227



### Authors
Jobson, BT
McKeen, SA
Parrish, DD
et al.



### Publication Date
1999-07-20

### DOI
10.1029/1999jd900126

JOURNAL OF GEOPHYSICAL RESEARCH, VOL. 104, NO. D13, PAGES 16,091-16,113, JULY 20, 1999

# Trace gas mixing ratio variability versus lifetime in the troposphere and stratosphere: Observations

B.T. Jobson,[1,2] S.A. McKeen,[1,2] D.D. Parrish,[3] FC. Fehsenfeld,[3] D.R. Blake,[4] A.H. Goldstein,[5] S.M. Schauffler,[6] and J.W. Elkins[7]

**Abstract.** Several archived data sets have been reviewed to examine the relationship between mixing ratio variability and lifetime for hydrocarbon and halocarbon species in the troposphere and stratosphere. The dependence on lifetime was described by the power law relationship $s_{\ln X} = A\tau^{-b}$, where $s_{\ln X}$ is the standard deviation of the ln of the mixing ratios, $A$ is a proportionality coefficient, and $b$ is an exponent that relates to the dominance of sink terms in the regional variability budget. At the Harvard forest ground site, winter and summer data displayed the same lifetime dependence, $\tau^{-0.18}$, which was significantly weaker than the $\tau^{-0.5}$ dependence of remote tropospheric data, indicating that source terms dominated regional variability at Harvard. In addition, the ratio of summer to winter $s_{\ln X}$ values was found to be similar for all species except ethane, averaging $1.54 \pm 0.04$. This ratio is consistent with a factor of 11 seasonal change in the species lifetimes, given a $\tau^{-0.18}$ lifetime dependence. Stratospheric data displayed a stronger lifetime dependence than tropospheric trends, indicating a more dominant role for sink terms in describing spatial variability in this region of the atmosphere. We show that a unique power law relationship between $s_{\ln X}$ ratios for two species $X_i$ and $X_j$ and the kinetic slope of $\ln(X_i)$ versus $\ln(X_j)$ correlation plots is found to hold in both observations and theory. Thus knowledge of the coefficient $b$ allows for a clearer understanding of the relationship between observed slopes of $\ln(X_i)$ versus $\ln(X_j)$ correlation plots and the ratio of the species lifetimes.

## 1. Introduction

The relationship between trace gas mixing ratio variability in the atmosphere and atmospheric lifetime has not been widely studied either from observations or from a theoretical standpoint. The most widely cited reference is *Junge* [1974], who found an empirical relationship between the global spatial variability of several trace gases in the troposphere and their steady state lifetimes. Junge's empirical relationship is

$$\mathrm{RSD} = \frac{0.14}{\tau} \quad (1)$$

where RSD is the relative standard deviation (the standard deviation divided by the mean concentration) and $\tau$ is the residence time in years. This relationship is often cited in the literature as it substantiates our intuitive notion that the more reactive trace gases are the more variable. The global spatial variability-lifetime relationship for the troposphere has been reexamined by *Jaenicke* [1982] and *Hamrud* [1983], and the updated data along with Junge's original data are shown in Figure 1. Over the years, lifetime estimates of several trace gases have changed substantially, but the inverse dependence on lifetime is still considered to be a reasonable fit through the data. This inverse dependence on lifetime has been reproduced in model studies by *Junge* [1974] and *Hamrud* [1983], although *Hamrud* [1983] concluded that the spatial relation between sources and sinks strongly influences trace gas spatial variability, with the $\tau^{-1}$ dependence only being approached for very long lived species.

*Jobson et al.* [1998] examined the variability-lifetime relationships for nonmethane hydrocarbons on a regional scale. They proposed using the standard deviation of the ln of the mixing ratios ($s_{\ln X}$) as the measure of variability rather than the relative standard deviation (RSD) used by *Junge* [1974] and others. For long lived species, which typically exhibit small variability, $s_{\ln X}$ is equivalent to RSD, but for short lived species like hydrocarbons, which may have standard deviations comparable to the mean mixing ratio, $s_{\ln X}$ gives much simpler behavior. The hydrocarbon data presented by *Jobson et al.* [1998] displayed strongly correlated $s_{\ln X}$ versus lifetime trends, although with a much weaker dependence on lifetime than the *Junge* [1974] relationship. This relationship is given by

$$s_{\ln X} = A\,\tau^{-b} \quad (2)$$

where $\tau$ is the lifetime and $A$ is a fitting parameter found in the regression fits to the data. The exponent $b$ takes on values between 0 and 1 and describes the importance of sink terms in the regional variability budget. In the 1993 North Atlantic Regional Experiment (NARE) the $C_2$-$C_4$ alkanes, acetylene, and benzene variability displayed an approximate $\tau^{-0.40}$ dependence [*Jobson et al.*, 1998]. These data were collected from ground sites and aircraft operating in July and August in

[1]Cooperative Institute for Research in Environmental Science, University of Colorado, Boulder, Colorado.
[2]Also at NOAA Aeronomy Laboratory, Boulder, Colorado.
[3]NOAA Aeronomy Laboratory, Boulder, Colorado.
[4]Department of Chemistry, University of California, Irvine.
[5]ESPM Ecosystems Sciences Division, University of California, Berkeley.
[6]National Center for Atmospheric Research, Boulder, Colorado.
[7]NOAA Climate Monitoring and Diagnostics Laboratory, Boulder, Colorado.



Paper number 1999JD900126.
0148-0227/99/1999JD900126$09.00

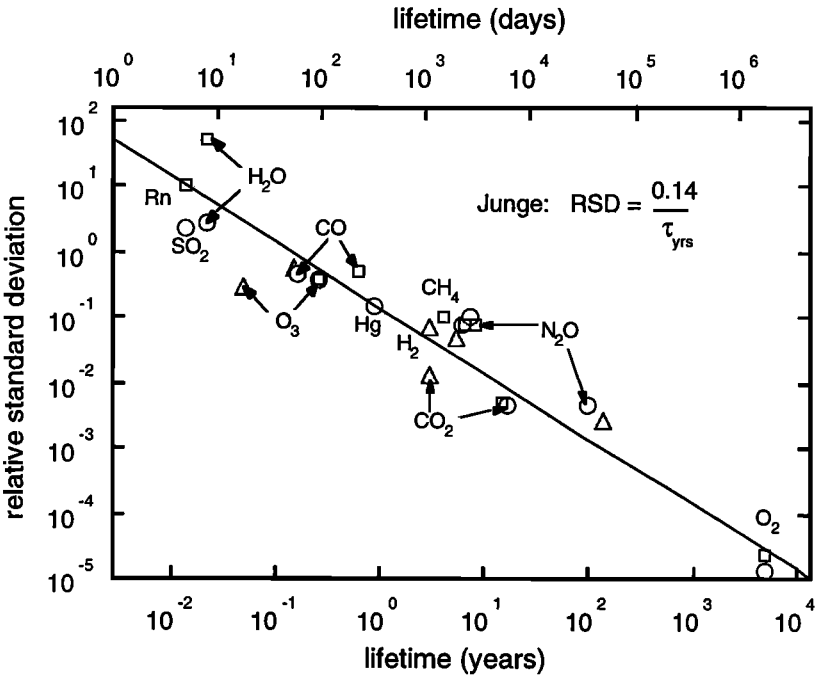


**Figure 1.** The original *Junge* [1974] plot (squares) with updates by *Jaenicke* [1982] (circles) and *Hamrud* [1983] (triangles).

maritime Canada and the western Atlantic. The variability in the NARE data was driven in part by the transport of urban pollution from large cities on the east coast of the United States and Canada. *Jobson et al.* [1998] also showed that wintertime hydrocarbon measurements from the Canadian arctic and Boulder, Colorado also displayed a strong though marginally weaker dependence on lifetime, $\sim\tau^{-0.30}$, and in areas strongly influenced by local sources, such as urban areas, no dependence on lifetime was observed. Recently, *Ehhalt et al.* [1998] examined variability-lifetime relationships using a three dimensional chemical tracer model and came to conclusions similar to those by *Jobson et al.* [1998]. They examined a relationship similar to (1) and found the dependence on $\tau$ to vary with geographic location. Within their model, continental source regions displayed a weaker $\tau$ dependence than remote ocean environments, and importantly, on a regional basis the lifetime dependence was much weaker than *Junge*'s [1974] inverse relationship.

The purpose of this paper is to extend the scope of *Jobson et al.* [1998] by including halocarbons and thus examine the robustness of the regional variability-lifetime relationship over a much broader lifetime range. In addition, stratospheric data will be examined with respect to (2) and compared to tropospheric trends. To our knowledge, tracer variability-lifetime relationships have not been examined in the stratosphere. The goal is to evaluate the exponent $b$ and thereby gain a better sense of the range of values it takes within the atmosphere. This exponent would appear to be a unique and important indicator for describing the dominance of sink terms on regional-scale tracer variability budgets [*Ehhalt et al.*, 1998]. We will show that knowledge of the value of $b$ allows for a straightforward relationship between the observed slopes of tracer correlation plots and the ratio of the species lifetimes.

This paper is a retrospective analysis of previously published data. In section 2.1, data from three of NASA's Global Troposphere Experiments (GTE) will be examined: the Arctic Boundary Layer Expedition 3B (ABLE 3B), the Transport and Atmospheric Chemistry Near the Equator - Atlantic (TRACE-A), and the Pacific Exploratory Mission in the Western Pacific Ocean Phase B (PEM-West B). The wide range of species and species lifetimes measured in these campaigns provides a good starting point for evaluating the robustness of the regional scale variability-lifetime relationship. In section 2.2, variability-lifetime relationships in the stratosphere from the Airborne Southern Hemisphere Ozone Experiment (ASHOE), the Airborne Arctic Stratospheric Expedition II (AASE II), and the Stratospheric Photochemistry Aerosols and Dynamics Expedition (SPADE) field campaigns will be examined. In section 2.3, seasonal differences in the trend will be discussed using hydrocarbon data from the Harvard forest experimental site [*Goldstein et al.*, 1995]. These data provide some unique additional insights into how the relationship in (2) can be used to infer seasonal changes in regional HO concentrations from tracer variability. In section 2.4 some data from the 1992 Polar Sunrise Experiment [*Jobson et al.*, 1994a] will be reexamined with respect to using variability-lifetime relationships to infer relative oxidant abundances.

The global atmospheric lifetime or residence time of a trace gas is defined as

$$\tau = \frac{\text{atmospheric burden}}{\text{atmospheric loss rate}} \tag{3}$$

Most of the gases considered here are removed in the troposphere through their reaction with the hydroxyl radical. The loss rate depends on the concentration of HO, which has pronounced temporal and spatial variability, the spatial

distribution of the trace gas, and the respective HO rate coefficient that may have a significant temperature dependence. Lifetimes are thus determined by a convolution of the spatial-temporal distribution of these three terms [*Prather and Spivakovsky*, 1990]. The loss rate and concentration of the trace gas $X$ at a particular location and time define the local lifetime

$$\tau_{local} = \frac{[X]}{k[HO][X]} = \frac{1}{k[HO]} \quad (4)$$

where $k$ is the HO rate coefficient and the square brackets indicate the concentration of the species of interest. Our previous analysis [*Jobson et al.*, 1998] examined the relative variability for hydrocarbons that were oxidized by HO exclusively. In that case the absolute value assumed for HO is unimportant in determining the coefficient $b$ in (2). However, in this study the variability of species lost by HO are compared with those lost by photolysis and the absolute value of lifetimes with respect to HO relative to those lost by photolysis must be considered. The tropospheric data analyzed here, with the exception of the Harvard forest data, were collected during field campaigns spanning no more than a month so that changes in mean concentrations of HO due to seasonal changes in insolation were negligible. In the analysis of the winter and summer hydrocarbon data from Harvard forest, estimates of the appropriate HO concentrations were obtained from chemical-transport models [*Goldstein et al.*, 1995].

For the GTE campaigns the range of HO reactivity for the gases considered is large, about a factor of 100, and we must consider whether local lifetimes or global mean lifetimes should be used in the analysis of regional variability-lifetime relationships. These studies used an aircraft as the sampling platform and sampled from a wide range of altitudes (from the near surface to 11 km) and latitudes. Gases with lifetimes greater than a year, such as $CH_3CCl_3$, are fairly evenly distributed through the troposphere. However, species with lifetimes of the order of days, such as acetylene and propane in summer, are oxidized rapidly in the boundary layer close to their emission sources. Boundary layer concentrations of HO are thus more important in determining the lifetimes of these hydrocarbons compared to longer lived gases. Accurately calculating the relative lifetimes of the gases considered here will be difficult, and we must accept a degree of uncertainty in our analysis. As discussed later, results are fairly insensitive to assumed HO levels for the more reactive hydrocarbons.

For species with lifetimes more than 100 days their mean global lifetimes were used. Estimates of the $CH_3CCl_3$ atmospheric lifetime inferred from measurements of the Atmospheric Lifetime Experiment (ALE) and Global Atmospheric Gas Experiment (GAGE) monitoring network [*Prinn et al.*, 1995] provide a reference lifetime to which other similarly long lived gases can be scaled [*Prather and Spivakovsky*, 1990]. Atmospheric lifetimes for the gases $CH_3Cl$ and $CH_3Br$ were scaled to the 4.9 year global mean lifetime of $CH_3CCl_3$ due to removal by HO according to *Prather and Spivakovsky* [1990]. The $CH_3Br$ lifetime also includes losses due to ocean uptake ($\tau$ = 3.7 years) and loss in the stratosphere ($\tau$ = 35 years) [*World Meteorological Organization (WMO)*, 1995]. Atmospheric lifetimes for $CCl_4$, chlorofluorocarbons (CFCs), hydrochlorofluorocarbons (HCFCs), and halons were taken from WMO [1995]. Atmospheric lifetimes of CFCs and $CCl_4$ are determined primarily by their photolysis rates in the stratosphere.

For species with lifetimes <100 days, such as hydrocarbons, haloalkenes, and short lived haloalkanes, local lifetimes were chosen. These were estimated using an average monthly HO concentration appropriate for the average latitude and time of year of the respective field campaigns [*Spivakovsky et al.*, 1990]. The HO concentrations at the 900 mbar level given by *Spivakovsky et al.* [1990] are similar enough for the different field experiments that a single representative HO concentration could be reasonably employed to calculate lifetimes for all three GTE field campaigns; we have assumed an average HO concentration of $1.3 \times 10^6$ molecules $cm^{-3}$ and calculated the rate coefficients at 288 K. These lifetimes serve as a reasonable starting point for the analysis of the data. Rate

**Table 1.** HO Rate Coefficients of Selected Species Used to Calculate Lifetimes

| Species | Rate Coefficient | Reference |
|---|---|---|
| *n*-Butane | $2.04 \times 10^{-17} T^2 \exp(85/T)$ | *Talukdar et al.* [1994] |
| *i*-Butane | $9.32 \times 10^{-18} T^2 \exp(275/T)$ | *Talukdar et al.* [1994] |
| Benzene | $3.58 \times 10^{-12} \exp(-280/T)$ | *Atkinson* [1994] |
| Propane | $1.01 \times 10^{-11} \exp(-660/T)$ | *Talukdar et al.* [1994] |
| Acetylene | $k_o = 5 \times 10^{-30} (T/298)^{-1.5}$<br>$k_\infty = 9.4 \times 10^{-12} \exp(-700/T)$<br>$F_c = \exp(-T/580) + \exp(2330/T)$ | *Atkinson* [1989] |
| Ethane | $1.03 \times 10^{-11} \exp(-1110/T)$ | *Talukdar et al.* [1994] |
| $C_2Cl_4$ | $9.64 \times 10^{-12} \exp(-1209/T)$ | *Atkinson* [1994] |
| $C_2HCl_3$ | $5.63 \times 10^{-13} \exp(427/T)$ | *Atkinson* [1994] |
| $CH_2Cl_2$ | $6.14 \times 10^{-18} T^2 \exp(-389/T)$ | *Atkinson* [1994] |
| $CHCl_3$ | $1.80 \times 10^{-18} T^2 \exp(-129/T)$ | *Atkinson* [1994] |
| $CH_3Cl$ | $7.33 \times 10^{-18} T^2 \exp(-809/T)$ | *Atkinson* [1994] |
| $CH_3Br$ | $3.62 \times 10^{-18} T^2 \exp(-711/T)$ | *Atkinson* [1994] |

**Table 2.** Lifetimes Used for GTE Data

| Species | Lifetime, days | Reference |
|---|---|---|
| *n*-Butane | 3.9 | local (288 K, 1.3 x $10^6$ OH) |
| *i*-Butane | 4.4 | local (288 K, 1.3 x $10^6$ OH) |
| Benzene | 6.6 | local (288 K, 1.3 x $10^6$ OH) |
| Propane | 8.7 | local (288 K, 1.3 x $10^6$ OH) |
| Acetylene | 13 | local (288 K, 1.3 x $10^6$ OH) |
| Ethane | 41 | local (288 K, 1.3 x $10^6$ OH) |
| $C_2HCl_3$ | 3.6 | local (288 K, 1.3 x $10^6$ OH) |
| $C_2Cl_4$ | 61 | local (288 K, 1.3 x $10^6$ OH) |
| $CH_2Cl_2$ | 67 | local (288 K, 1.3 x $10^6$ OH) |
| $CHCl_3$ | 93 | local (288 K, 1.3 x $10^6$ OH) |
| $CH_3Cl$ | 358 | scaled to $CH_3CCl_3$ |
| $CH_3Br$ | 360 | *WMO* [1995], chap. 10 |
| $CH_3CCl_3$ | 1,750 | *Prinn et al.* [1995] (global) |
| $CCl_4$ | 15,300 | 42 years *WMO* [1995] |
| CFC-11 ($CCl_3F$) | 18,300 | 50 years *WMO* [1995] |
| CFC-113 ($CCl_2FCClF_2$) | 31,000 | 85 years *WMO* [1995] |
| CFC-12 ($CCl_2F_2$) | 37,300 | 102 years *WMO* [1995] |
| CFC-114 | 110,000 | 300 years *WMO* [1995] |
| HCFC-22 | 4,860 | 13.3 years *WMO* [1995] |
| H-1211 | 7,300 | 20 years *WMO* [1995] |
| H-1301 | 23,700 | 65 years *WMO* [1995] |

GTE, Global Troposphere Experiment; WMO, World Meteorological Organization.

coefficients used to calculate lifetimes are given in Table 1, and the resulting lifetimes are given in Table 2.

## 2. Results

### 2.1. Tropospheric Data

In this section the regional trends from the ABLE 3B, TRACE-A, and PEM-West B field experiments will be discussed. All three experiments were aircraft-based field campaigns sponsored by NASA, pertinent details of which are given in Table 3. More detailed information can be found in the overview papers of the specific experiments: ABLE 3B [*Harriss et al.*, 1994], TRACE-A [*Fishman et al.*, 1996], and PEM-West B [*Hoell et al.*, 1997]. Each experiment had specific objectives, so aircraft flight plans were not designed for a random sampling of the atmosphere. The trace gas distributions therefore reflect the sampling bias inherent to the mission objectives. The data from these experiments were obtained by the same research group so there is internal consistency amongst the various experiments. In general, the samples were collected from aircraft over relatively remote regions of the Northern and Southern Hemispheres with some sampling of air that had been recently influenced by urban and biomass burning sources. Overall, the trace gas distributions should be representative of reasonably well processed anthropogenic and natural emissions.

Figure 2 illustrates the influence of fresh urban emissions and stratospherically influenced air for some hydrocarbon and

**Table 3.** Details of the Field Experiments

| | ABLE 3B | TRACE-A | PEM-West B | AASE-II | SPADE | ASHOE |
|---|---|---|---|---|---|---|
| Date | July - August 1990 | September -October 1992 | February - March 1994 | October 1991 to March 1992 | May 1993 | March - November 1994 |
| Platform | NASA Electra | NASA DC-8 | NASA DC-8 | NASA ER2 | NASA ER2 | NASA ER2 |
| Geographic area | troposphere: Hudson Bay lowlands, northern Quebec | troposphere: south Atlantic, Brazil, southern Africa | troposphere: western Pacific | stratosphere: Northern Hemisphere 15°N-90°N | stratosphere: Northern Hemisphere 15°N-60°N | stratosphere: Southern Hemisphere 20°N-69°S |
| Altitude Range | PBL to 6 km | PBL to 12 km | PBL to 12 km | 17-20 km | 17-20 km | 17-20 km |
| Data used | UCI cans flights 2-20 | UCI cans flights 5-17 | UCI cans flights 4-19 | NCAR cans | CMDL in situ gas chromatograph | CMDL in situ gas chromtagraph |
| Samples | 749 | 1267 | 2041 | 468 | 709 | 1519 |
| Study focus | biomass burning and transport from cities | biomass burning in Brazil and Africa | outflow of anthropogenic emissions from Asia | Arctic vortex | seasonal and latitudinal distribution of trace gases | seasonal and latitudinal distribution of trace gases |

ABLE 3B, Arctic Boundary Layer Expedition 3B; TRACE-A, Transport and Atmospheric Chemistry Near the Equator - Atlantic; PEM West B, Pacific Exploratory Mission in the Western Pacific Ocean Phase B; AASE II, Airborne Arctic Stratospheric Expedition II; SPADE, Stratospheric Photochemistry Aerosols and Dynamics Expedition; ASHOE, Airborne Southern Hemisphere Ozone Experiment; PBL, planetary boundary layer; UCI, University of California Irvine; NCAR, National Center for Atmospheric Research; CMDL, NOAA Climate Monitoring and Diagnostics Laboratory.

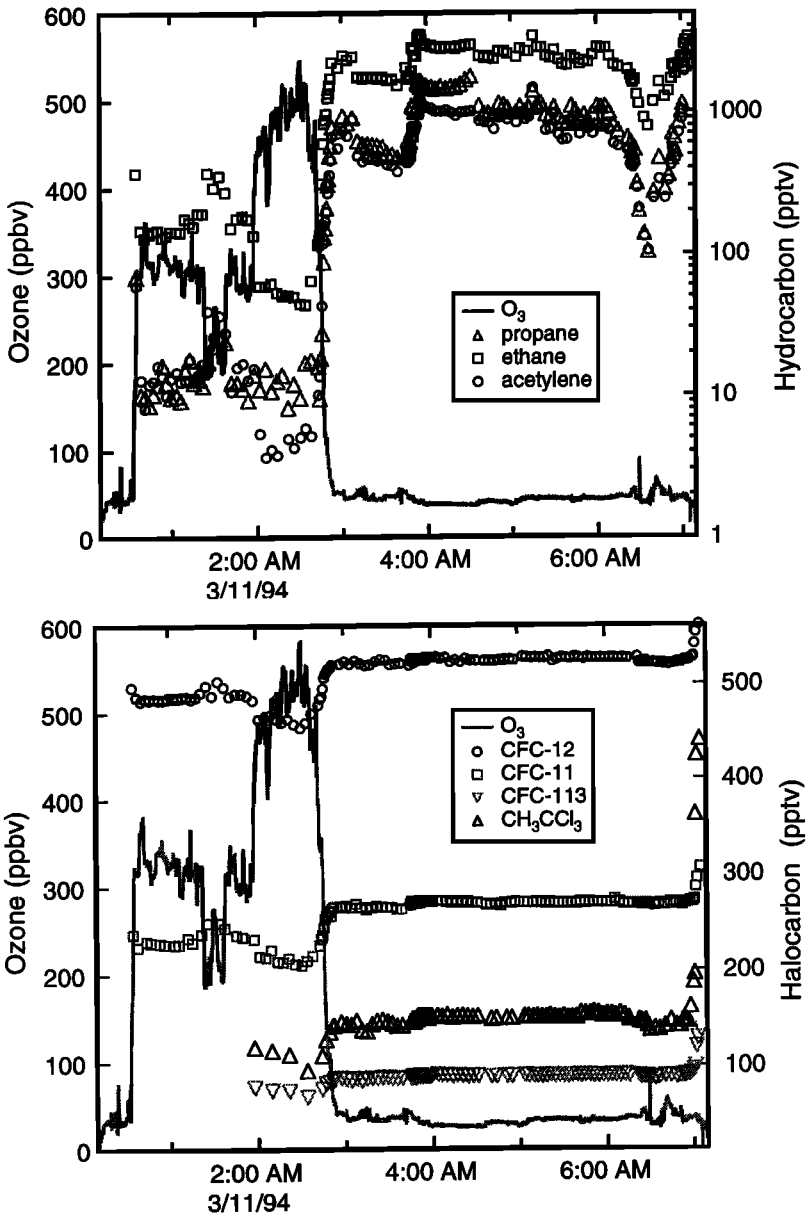


**Figure 2.** Stratospheric intrusion (0030-0300 UT) and urban plume data (after 0700 UT) from the mission 17 flight of the Pacific Exploratory Mission in the Western Pacific Ocean Phase B (PEM-West B) illustrating the influence of these air masses on trace gas distributions.

chlorofluorocarbon mixing ratios. These two types of air masses defined the maximum and minimum of the mixing ratio distributions for many species. The data were collected during mission 17 of the PEM-West B experiment. The urban samples are evident at the end of the flight just after 7 am UT, taken as the plane descended through the urban plume of Yokota, Japan, to the airport. Typically, $O_3$ was very depleted when these samples were taken, reflecting the large NO concentration that was likely present (the NO instrument did not sample during these approaches to prevent inlet contamination). These few "airport" samples, from this flight and others, strongly influenced the variability of the long-lived gases such as $CH_3CCl_3$ and the CFCs because of their extremely elevated mixing ratios relative to regional levels. For example, $CH_3CCl_3$ mixing ratios in this plume were up to 3 times higher than the campaign average. Such samples were not included in the analysis of the GTE data since they are unrepresentative of processed tropospheric air. Also not included were samples collected during the transit flights to and from the study region for the ABLE 3B and TRACE-A experiments.

The stratospherically influenced air in Figure 2 is indicated by elevated ozone mixing ratios up to 500 ppbv and depleted mixing ratios of hydrocarbons and the very long lived gases such as CFC-11 and CFC-12. Samples collected in stratospheric intrusions were included in the analysis. These data comprise a small percentage of the total data set, but the stratospheric intrusions are included as an important general

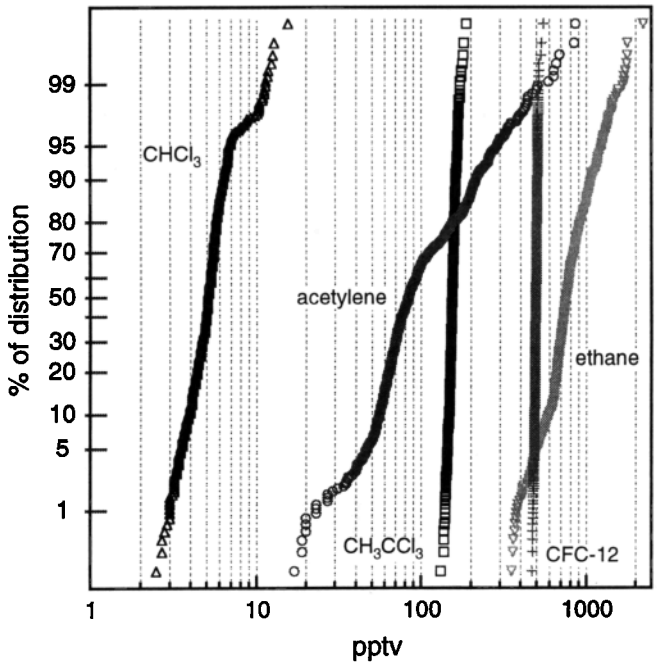


**Figure 3.** Cumulative distributions of selected trace gases measured in Arctic Boundary Layer Expedition 3B (ABLE 3B).

process in shaping mixing ratio distributions in the troposphere by injecting photochemically processed air and hence low mixing ratios of these trace gases, particularly for CFCs.

**2.1.1. Statistical distributions.** The statistical distributions of the trace gases measured in the GTE experiments tended to become more skewed or approximately lognormal as the reactivity of the species increased. To illustrate this point, Figure 3 shows the cumulative distribution of several species measured in ABLE 3B. These gases span a lifetime range from ~10 days for acetylene to ~40,000 days for CFC-12. There is a clear tendency for the dynamic range to increase with increasing reactivity. In these logarithmic cumulative distribution plots, lognormal distributions define straight lines. Taking the natural log of the mixing ratios transforms the distributions into a more symmetric form so that the character of the distributions are more comparable across the large lifetime range of these gases. Figure 4 compares histograms of the ln of the mixing ratios for several trace gases. For most species these distributions can be approximated by a Gaussian probability density function, but some species distributions are more complex. For example, ln(acetylene) is not well described by a Gaussian distribution; the Pem-West B data is bimodal, while the ABLE 3B and TRACE-A data display distinct shoulders. Thus $s_{\ln X}$ may not be the perfect statistic for comparing relative variability amongst these gases, but as the following figures attest, it is sufficient for capturing the general trends in the data.

**2.1.2. Variability versus lifetime.** Figure 5 displays the relationship between $s_{\ln X}$ versus lifetime for the ABLE 3B, TRACE-A, and PEM-West B data. Individual flights displayed the same trends to a greater or lesser degree. In general, though, there was much more scatter in the trends of individual flights. The $s_{\ln X}$ value was calculated from all the samples collected from the flights indicated in Table 3. Some species did not have 100% data coverage because of being below detection limits or other analytical problems. For the $C_4$ and higher alkanes, no data were reported for a large fraction of the collected samples in all three field campaigns. The variability statistics for these species would be biased low relative to species with complete quantitation of their spatial distribution. Species with a significant fraction of unreported data (>11%) were not included in the analysis. Table 4 lists the $s_{\ln X}$ values and the percentage of missing data for each of the field missions. In general, the data from these field missions define a relatively coherent relation between $s_{\ln X}$ and lifetime of the form $s_{\ln X} = A\ \tau^{-b}$, with the exponent $b$ approximately equal to 0.5. Some species were clearly outliers to the general trend and were not included in the regression fit. These outliers will be discussed below in terms of differences in trace gas source distributions and emissions history. Table 5 lists the fit parameters and the associated 1σ uncertainties. The parameter values were found from a linear regression of $\ln(s_{\ln X})$ versus ln(lifetime). As compared to an exponential fit, the linear regression of the ln transformed data yielded more reliable estimates of the uncertainties for $A$ and $b$, particularly for the GTE data where the lifetimes spanned 4 orders of magnitude. In Figure 5a two other fits are shown by dashed lines to illustrate the uncertainty associated with the estimated local lifetimes. Using an HO concentration of 1 x $10^6$ molecules $cm^{-3}$ resulted in a $\tau^{-0.44}$ dependence, while an HO concentration of 2 x $10^6$ yielded a $\tau^{-0.48}$ dependence. This range of lifetime dependencies is within the 1σ uncertainty in the lifetime dependence in Table 5.

**2.1.3. General trace gas sources.** For the most part the species in Figures 5 are associated with anthropogenic emissions from fossil fuel use, solvent use, and industrial processes. The one exception is $CH_3Cl$, which is not thought to have strong urban or industrial sources but does have a significant oceanic source [*Singh et al.*, 1983]. Many species are also emitted from burning biomass, in particular, hydrocarbons [*Blake et al.*, 1994] and simple haloalkanes such as $CH_3Cl$, $CH_3Br$, and $CH_2Cl_2$ [*Rudolph et al.*, 1995; *Blake et al.*, 1996]. Biomass burning is not a significant source of CFCs, $CCl_4$ and $CH_3CCl_3$ compared to urban and industrial emissions [*Rudolph et al.*, 1995]. Biomass burning was an important hydrocarbon source in ABLE 3B, where more than 50% of the vertical profiles flown displayed hydrocarbon mixing ratio enhancements due to forest fire plumes [*Blake et al.*, 1994]. *Wofsy et al.* [1994a] estimated that forest fires were a larger source input than long range transport of urban and industrial emissions in shaping regional hydrocarbon mixing ratios. Biomass burning also appeared to be an important trace gas source in the TRACE-A experimental region [*Gregory et al.*, 1996; *Talbot et al.*, 1996; *Fishman et al.*, 1996]. Biomass burning was a less significant contributor to the general trace gas source distribution in PEM-West B, which was influenced primarily by urban and industrial emissions from the Asian continent [*Talbot et al.*, 1997; *Gregory et al.*, 1997]. The good relationship between hydrocarbons that had large biomass burning sources in ABLE 3B and TRACE-A and the haloalkanes and CFCs which do not have significant biomass burning sources is notable. The coherence of the variability-lifetime trend appears to be insensitive to the degree of source collocation. The relationship must reflect a general pattern that develops as a result of dispersion and removal of trace gases from area or point sources on continents.

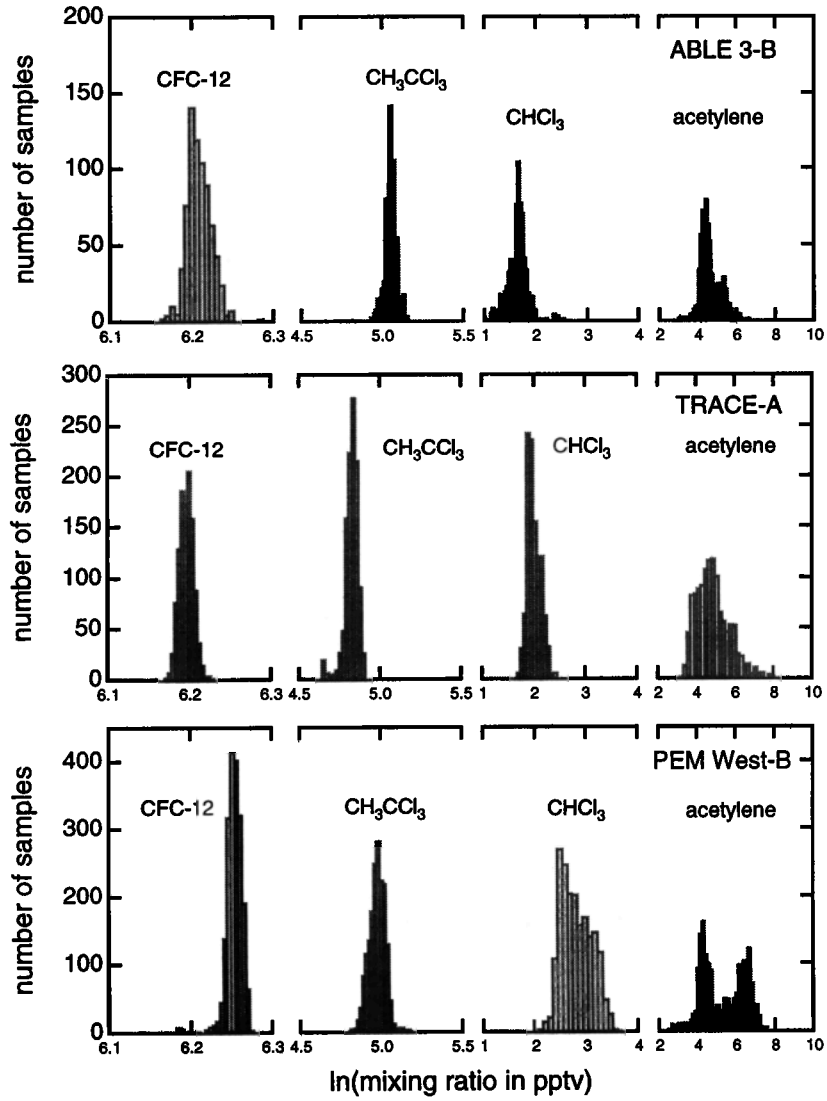


**Figure 4.** Histograms of the ln of the mixing ratios of selected trace gases measured in ABLE 3B, Transport and Atmospheric Chemistry Near the Equator - Atlantic (TRACE-A), and PEM-West B.

**2.1.3.1. $CH_3Cl$:** It is evident that $CH_3Cl$ is a significant outlier in the PEM-West B data set. This is likely due to its much different source distribution. *Blake et al.* [1997] have noted that the spatial distribution of its mixing ratio was significantly different from that of the other species, likely a result of the large distributed emission source from the Pacific Ocean. A large distributed emission source would result in a smaller spatial variability than gases of urban or industrial origin that are transported in regional plumes originating from Asia. In the TRACE-A data set, $CH_3Cl$ also displays a lower variability than the general trend but to a smaller extent. The better fit is likely due to the larger contribution of biomass burning as a $CH_3Cl$ source, which made its emission distribution more like the other trace gases plotted. Because $CH_3Cl$'s source distribution can be significantly different than the other gases, it was not used in the regression fits shown in Figure 5.

**2.1.3.2. CFC-114, H-1211, and H-1301:** These species displayed significantly higher variability than the general trend. The measured spatial variability is greater than the estimated measurement precision (although the measurement variances do contribute to the observed variability). These species are anthropogenic in origin, and there is no reason to believe that their source distribution is significantly different than that of the other CFCs. The high spatial variability of these species with respect to the other similarly long lived CFCs is likely a consequence of their much lower regional mixing ratios. Their lower mixing ratios are a result of their historical emission rates being a factor of 10 or more lower than those of CFC-11, CFC-12, CFC-113, and HCFC-22 [*Kaye et al.*, 1994]. We can imagine this effect arising as follows. Assume that the variability of species $X_i$ in some region is driven by pollution plumes from an anthropogenic source. With steady emissions the ratio between plume concentrations and the average regional background will decrease as $X_i$ accumulates in the atmosphere. Therefore the spatial and temporal variability, as described by $dX_i/X_{i,avg}$ will decrease with time until $X_i$ is in steady state with respect to loss and production. One might anticipate that with continued emissions and increasing global concentrations of these species

that their spatial variability will decrease and become a better fit to the regional trend. If the regional variability of these species is dominated by source terms, then they will exhibit a weaker $\tau$ dependence than the general trend.

### 2.2. Stratospheric Data

The variability lifetime relationships from the ASHOE, AASE II and SPADE field campaigns were examined. Pertinent details of these field experiments are given in Table 3. Further details can be found in the overview papers: ASHOE, *Tuck et al.* [1997]; AASE II, *Anderson and Toon* [1993]; SPADE, *Wofsy et al.* [1994b]. Data from the ASHOE experiment have been discussed by *Volk et al.* [1997] and have stated the $1\sigma$ measurement precision to be ~3% for most of the gases sampled. Further experimental details are given in *Elkins et al.* [1996]. *Woodbridge et al.* [1995] have discussed the AASE II data. In our analysis, only stratospheric samples were included. These samples were identified by a potential temperature greater than 400 K.

Figure 6 shows histograms of the ln transformed data for several selected species measured in the three field missions.

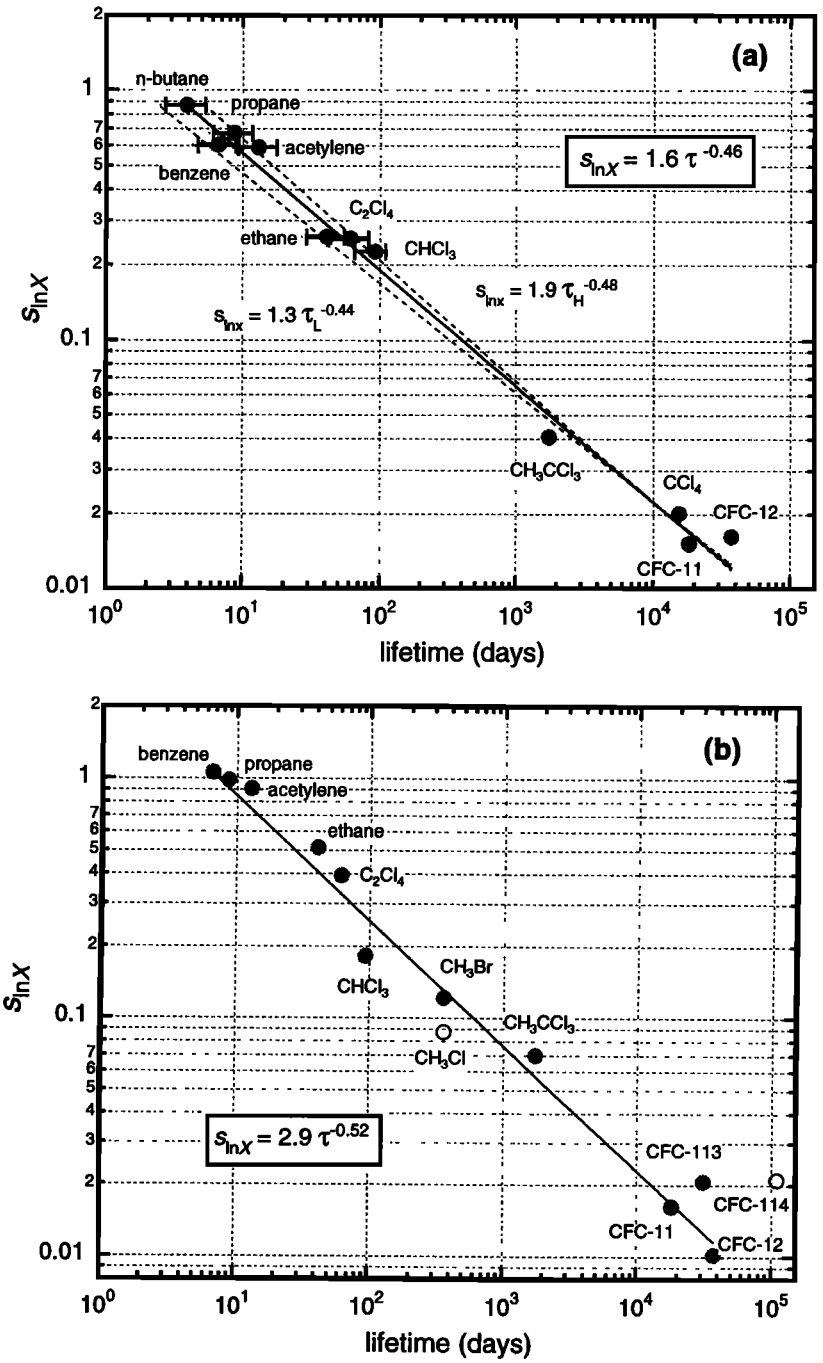


**Figure 5.** (a) ABLE 3B $s_{lnX}$ versus atmospheric lifetime. Dashed lines are fits using lower and upper estimates of local lifetimes for hydrocarbons as indicated by the error bars. (b) TRACE-A $s_{lnX}$ versus atmospheric lifetime. (c) PEM-West B $s_{lnX}$ versus atmospheric lifetime. Open circle data were not included in the regression fits to the TRACE-A and PEM-West B data.

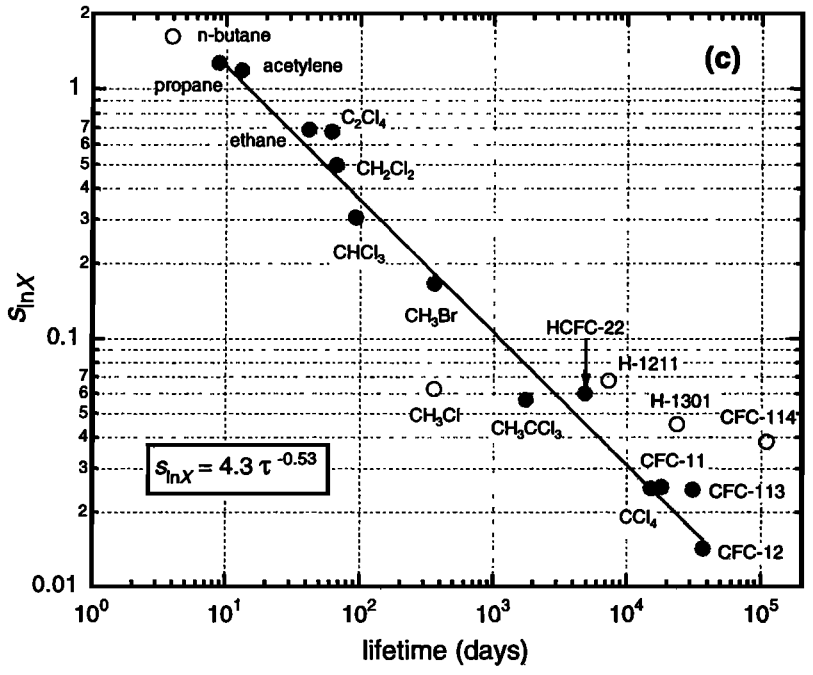


**Figure 5.** (Continued)

The ASHOE data display a bimodal statistical distribution, with both modes being reasonably symmetric. A narrow peak is evident in the distribution at high mixing ratios for all species. This mode corresponds to data collected in the tropics. The other mode is much broader and corresponds to samples collected in the extratropics. The SPADE data are also reasonably symmetric, but a minor mode or tail is evident at low mixing ratios. The AASE II data have a significant tail at low mixing ratios and the ln-transformed data are much less symmetric than the ASHOE or SPADE data.

Plate 1 shows $s_{lnX}$ versus the global steady state lifetime due to stratospheric loss for a number of species. The data are from the October 13 flight of the ASHOE mission where 93 stratospheric air samples were collected. This flight traversed a latitude range from 43° S to 68° S and thus sampled extratropical air. Shown are a number of different recommendations for tracer lifetimes and some corresponding regression fits. The lifetimes used in Plate 1 are defined as

$$\tau = \frac{\text{atmospheric burden}}{\text{stratospheric sink}} \quad (5)$$

The WMO/Intergovernmental Panel on Climate Change (IPCC) lifetimes shown in Plate 1 are taken from *Volk et al.* [1997] who used two different tracer correlation techniques to estimate stratospheric lifetimes. *Volk et al.* [1997] used a subset of the ASHOE data (they used data collected in the lowermost stratosphere) to estimate lifetimes from tracer correlations with CFC-11 and an assumed CFC-11 lifetime and a separate approach that related tracer gradients at the extratropical tropopause with $SF_6$ based estimates of air parcel age. The *Avallone and Prather* [1997] lifetimes are based upon a 3-D chemical transport model and used the AASE II data set as a comparison of model performance.

Plate 1 illustrates several points. First, stratospheric trends from individual flights were typically much more coherent and more similar to the overall trend in the respective field campaigns than the tropospheric data. Second, there is significant uncertainty in estimated lifetimes of individual species and in their relative lifetimes, as reflected in the wide spread of recommended lifetimes for individual species. Third, the relative stratospheric lifetimes are much different than their atmospheric lifetimes shown in Figure 5. For example, $CH_3CCl_3$ and $CCl_4$ are considered to have similar stratospheric lifetimes but have very different atmospheric lifetimes because $CH_3CCl_3$ is consumed relatively rapidly in the troposphere by reaction with the HO radical. In the troposphere, $CH_3CCl_3$ is much more variable than $CCl_4$, but in the stratosphere they displayed similar variability. Another example is methane, which has a shorter atmospheric lifetime than $N_2O$, again because of its relatively rapid consumption in the troposphere by the HO radical, but is considered to have a comparable stratospheric lifetime. In the data we have examined, methane always displayed a lower variability than $N_2O$ in the stratosphere, suggesting that its stratospheric lifetime should be longer. The *Avallone and Prather* [1997] lifetimes for $CH_4$ and $N_2O$ are consistent with this observation. The other lifetime estimates have the $CH_4$ lifetime being equal to or less than that of $N_2O$.

The lifetimes that are probably the most uncertain are those of $CH_3CCl_3$, $CH_4$, and $CH_3Cl$. These lifetimes are difficult to define in terms of stratospheric loss because of differences in the stratosphere-troposphere division between models. This leads to differences in the calculated lifetimes because these particular species have a significant HO removal rate (which is sensitive to $H_2O$ concentrations) whereas the other species are removed primarily by photolysis higher up in the atmosphere. For this reason we will exclude these species from the regression fits of the $s_{lnX}$ versus $\tau$ trends. In Plate 1 the regression fits for three lifetime recommendations are shown as the solid lines, the dashed lines being an extrapolation over the x axis lifetime range. Of the five recommendations, the *Avallone and Prather* [1997] and the WMO/IPCC lifetimes displayed the most coherent trend, both having an $r^2 = 0.993$. Two of the recommendations, *Kaye et al.* [1994] and the

**Table 4.** The $s_{\ln X}$ Values and Percentage of Missing Data for the GTE Field Campaigns Shown in Figure 5

| | ABLE 3B | | TRACE - A | | PEM - West B | |
|---|---|---|---|---|---|---|
| Species | $s_{\ln X}$ | % Missing | $s_{\ln X}$ | % Missing | $s_{\ln X}$ | % Missing |
| *n*-Butane | 0.868 | 11 | | 27 | 1.63 | 25 |
| *i*-Butane | 0.663 | 43 | | 49 | 1.36 | 37 |
| Benzene | 0.602 | 2 | 1.06 | 6.7 | | 99 |
| Propane | 0.671 | 0.1 | 0.981 | 0.8 | 1.27 | 1 |
| Acetylene | 0.590 | 0 | 0.900 | 0.6 | 1.19 | 1 |
| Ethane | 0.259 | 0.1 | 0.514 | 0.5 | 0.686 | 1 |
| $C_2HCl_3$ | | | | | 0.825 | 7 |
| $C_2Cl_4$ | 0.254 | 0.4 | 0.393 | 11 | 0.674 | 6 |
| $CH_2Cl_2$ | | | | | 0.497 | 3 |
| $CHCl_3$ | 0.226 | 0.3 | 0.182 | 15 | 0.306 | 6 |
| $CH_3Cl$ | | | 0.0876 | 0.2 | 0.0628 | 2 |
| $CH_3Br$ | | | 0.121 | 0.5 | 0.167 | 2 |
| $CH_3CCl_3$ | 0.0408 | 0.3 | 0.0700 | 10 | 0.0566 | 11 |
| $CCl_4$ | 0.0201 | 0.3 | | | 0.0248 | 11 |
| CFC-11 | 0.0152 | 0.3 | 0.0162 | 10 | 0.0252 | 2 |
| CFC-113 | | | 0.0207 | 10 | 0.0245 | 7 |
| CFC-12 | 0.0162 | 0.3 | 0.0102 | 10 | 0.0142 | 2 |
| CFC-114 | | | 0.0211 | 10 | 0.0384 | 2 |
| HCFC-22 | | | | | 0.0601 | 3 |
| H-1211 | | | | | 0.0676 | 2 |
| H-1301 | | | | | 0.0450 | 0.5 |

WMO/IPCC lifetimes adopted from *Volk et al.* [1997], yielded a value of $b$ larger than unity, 1.53 ± 0.12 and 1.25 ± 0.06, respectively. A $b$ value >1 is inconsistent with the behavior expected for the simple interaction of first-order removal processes and mixing. The Volk et al. [1997] lifetime estimates yielded $b$ values <1, although with a greater uncertainty than the fit through the *Avallone and Prather* [1997] recommendations. The $SF_6$ air mass age method yielded $b$ = 0.99 ± 0.15 and the CFC-11 correlation technique yielded $b$ = 0.98 ± 0.16.

The *Avallone and Prather* [1997] chemical transport model based lifetimes yielded the most coherent relationship between variability and lifetime in the stratospheric data sets we examined, and in all cases with $b$ values ≤1.0. In particular, the difference in the $N_2O$ and $CH_4$ lifetimes given by *Avallone and Prather* [1997] is consistent with observed differences in the variability of these species, though as stated before, we will not use $CH_4$ in the analysis that is to follow. Given the better overall fit to the data, we will use the Avallone and Prather stratospheric lifetimes for evaluating the variability-lifetime relationship. Our intent is to contrast the $b$ value of the stratospheric data trends with those of the troposphere; thus any of the recommendations could have been used in the analysis and would not have changed the general conclusions drawn.

The timescale for photochemical removal in the stratosphere is defined in terms of the stratospheric burden

$$\tau_{strat} = \frac{\text{stratospheric burden}}{\text{stratospheric sink}} \quad (6)$$

This is the timescale of interest for investigating variability-lifetime relationships in the stratosphere. The stratospheric burden is ~10% of the atmospheric burden for a well-mixed long-lived gas such as $SF_6$, so the stratospheric lifetime defined by (6) is ~10% of the value defined by (5). For shorter-lived species with mixing ratio profiles that fall off rapidly with height in the stratosphere their burden will be less than the 10% mass fraction factor. This fraction could be calculated

**Table 5.** Fit Parameters to $\ln(s_{\ln X}) = \ln(A) - b \ln(t)$

| | $A$ | $b$ |
|---|---|---|
| ABLE 3B | 1.6 ± 0.15 | 0.46 ± 0.02 |
| TRACE-A | 2.9 ± 0.44 | 0.52 ± 0.02 |
| PEM-West B | 4.3 ± 0.63 | 0.53 ± 0.02 |
| ASHOE tropical: | | |
| October | 0.17 ± 0.02 | 0.74 ± 0.07 |
| March, April, and May | 0.56 ± 0.11 | 0.62 ± 0.11 |
| ASHOE extratropical | 1.6 ± 0.18 | 0.97 ± 0.06 |
| AASE II | 3.3 ± 0.32 | 0.90 ± 0.05 |
| SPADE tropical | 0.37 ± 0.04 | 0.57 ± 0.06 |
| SPADE extratropical | 1.0 ± 0.03 | 0.68 ± 0.01 |
| Harvard forest | 0.99 ± 0.45 | 0.18 ± 0.16 |
| PSE 1992 ice island | 3.2 ± 0.32 | 0.92 ± 0.04 |

PSE, Polar Sunrise Experiment.

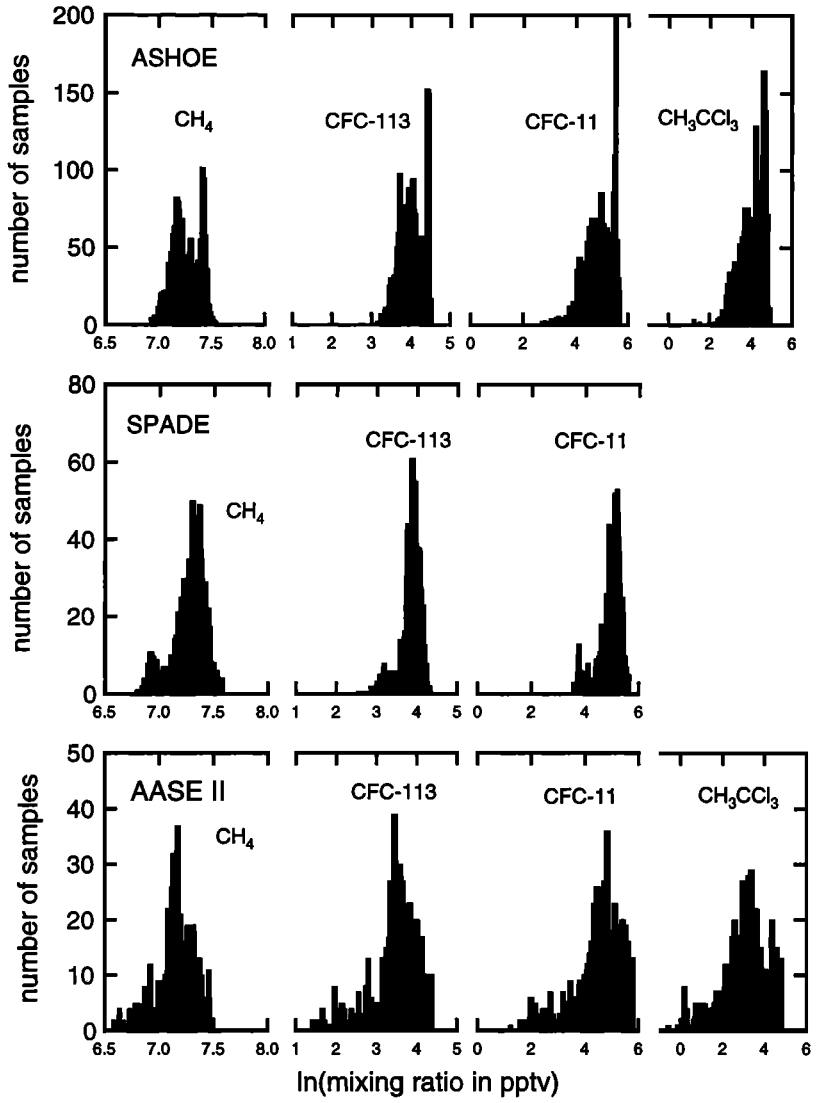


**Figure 6.** Histograms of ln of the mixing ratios for selected species measured in Airborne Southern Hemisphere Ozone Experiment (ASHOE), Stratospheric Photochemistry Aerosols and Dynamics Expedition (SPADE), and Airborne Arctic Stratospheric Expedition (AASE II).

with chemical transport models, but to simplify our analysis, we will apply the 10% fraction to all species so that the lifetimes shown in Plate 1 will be divided by 10 in Figures 7, 8, and 9. Applying the same factor to all species will bias our lifetime distribution somewhat, resulting in $b$ values biased high. However there is some practical advantage to using the same factor because the $b$ values determined from plots using the lifetime definition in (5) will be the same as those using the definition in (6), and gaining a general understanding of how $b$ varies between atmospheric regions is our primary goal. Of course, the choice of lifetime definitions will dramatically influence the value obtained for the proportionality coefficient $A$. The meaning of this coefficient will be briefly discussed for stratospheric data in section 3 where it will become more obvious why $s_{\ln X}$ should be plotted against the lifetime definition given in (6).

It is apparent in the histograms of the ASHOE data that the tropical and extratropical data defined different statistical distributions, and it is informative to plot these data separately. Figure 7a shows the relationship between $s_{\ln X}$ and lifetime for the tropical data divided into two periods on the basis of the large difference in the variability of the measurements. The late October flights displayed less variability than flights flown early in the year. Despite the large differences in variability the two periods displayed a similar lifetime dependence given the uncertainty in the exponent $b$. This dependence is stronger than that observed in the troposphere, and the data contain a clear stratospheric processing signature since $CCl_4$ and $CH_3CCl_3$ displayed similar variability. The ASHOE extratropical data in Figure 7b displayed a stronger lifetime dependence than the tropical data; $b$ is not significantly different than unity.

Figures 8 and 9 show the relationship between $s_{\ln X}$ and stratospheric lifetime for the AASE II and SPADE data sets. These data were primarily collected from the extratropics of the Northern Hemisphere. Because there are only three data points in Figure 9, we have included methane in the regression fit. The fit parameters to these and the ASHOE trends are given

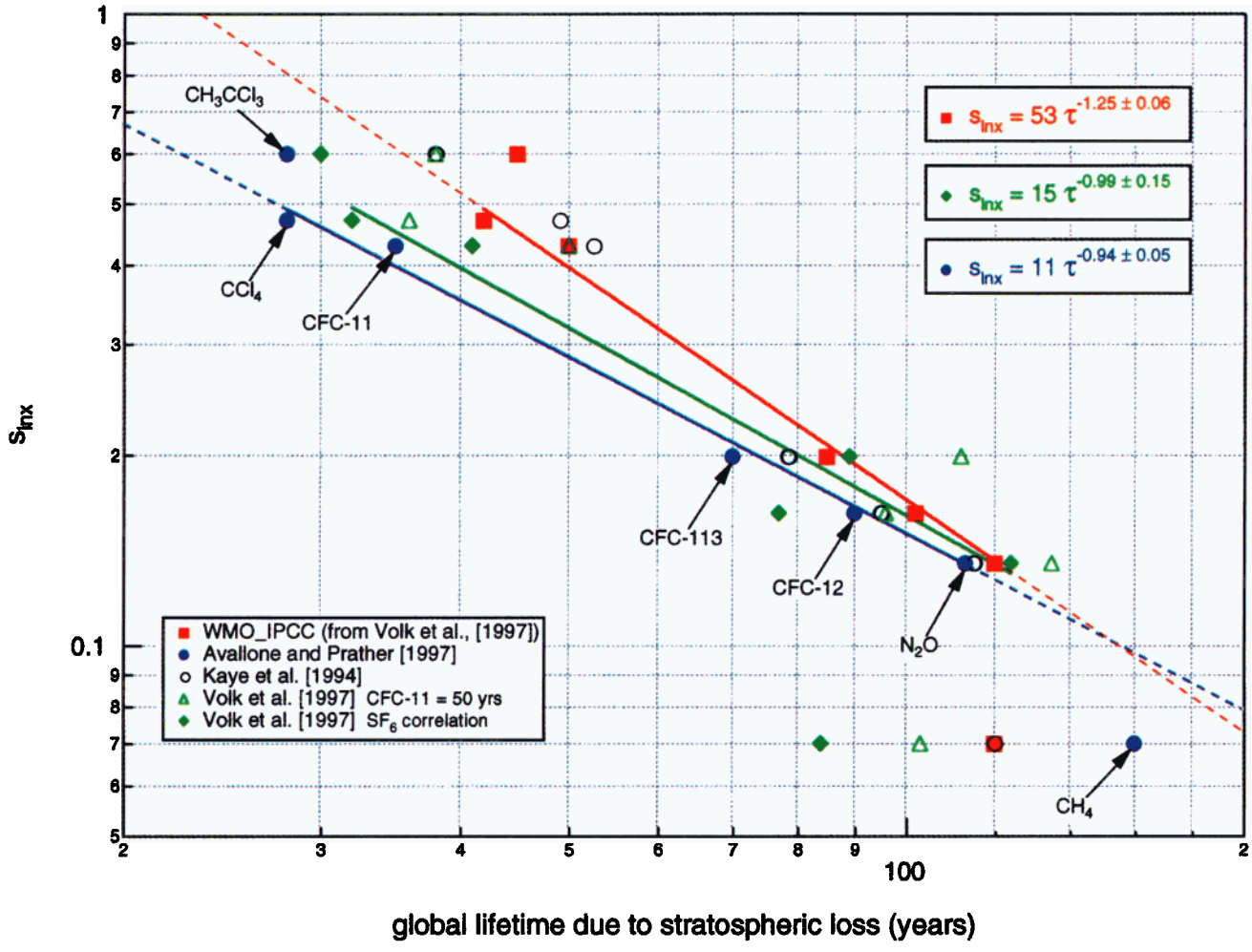


**Plate 1.** The $s_{lnX}$ versus global lifetime due to stratospheric loss for the ASHOE October 13 flight showing different recommended values of tracer lifetimes.

in Table 5. Data from the AASE II field campaign displayed a coherent trend although more scattered than the ASHOE data. In particular $CH_3Cl$ and $CH_4$ displayed much lower variability than the general trend. There is no reason to believe that $CH_3Cl$ should not fit the trend line since the source geometry for these trace gases in the stratosphere is the same, tropospheric air entering through the tropical tropopause. The reason for the outlying nature of $CH_3Cl$, $CH_4$, and to a lesser extent, $CH_3CCl_3$ is not clear but may be due to an overestimation of their HO removal rates by the *Avallone and Prather* [1997] model for this particular data set. Overall a greater range of mixing ratios was measured in AASE II, and accordingly, values of $s_{lnX}$ are larger than those in ASHOE and SPADE. The AASE II data displayed a lifetime dependence that is marginally weaker than the ASHOE extratropical data. Interestingly, the extratropical SPADE data from the month of May displayed a weaker $\tau$ dependence than the AASE II or ASHOE data. Data from individual flights and for the entire SPADE mission displayed an $\sim\tau^{-0.7}$ dependence, resembling the tropical data of ASHOE, but the variability in SPADE was somewhat greater. One flight from SPADE in the month of May collected data from the tropics, and this trend is shown separately in Figure 9. The lifetime dependence is slightly weaker than the other SPADE flights in May and is similar to the approximate $\tau^{-0.50}$ dependence of the tropospheric data, although the variability of the CFCs is still about an order of magnitude greater in the stratosphere than the troposphere.

### 2.3. Harvard Forest Seasonal Trends

So far, we have been looking at different data sets with the aim to understand better the physical significance of the lifetime dependence. For short-lived species such as hydrocarbons, seasonal changes in insolation drive a significant change in local lifetimes and hence large seasonal changes in mixing ratios [*Klemp et al.*, 1997; *Young et al.*, 1997; *Goldstein et al.*, 1995, *Jobson et al.*, 1994a; *Penkett et al.*, 1993; *Blake and Rowland*, 1986; *Singh and Salas*, 1982]. *Jobson et al.* [1998] noted that winter data displayed a weaker dependence than summer, but those data were collected from widely scattered locations. The Harvard forest data offer the opportunity to examine quantitatively seasonal changes in the regional lifetime dependence.

Plate 2 shows the summer (June, July, and August) and winter (December, January, and February) cumulative distributions of several hydrocarbon species measured at the Harvard forest experimental site by *Goldstein et al.* [1995]. The differences in winter and summer mixing ratios are largely

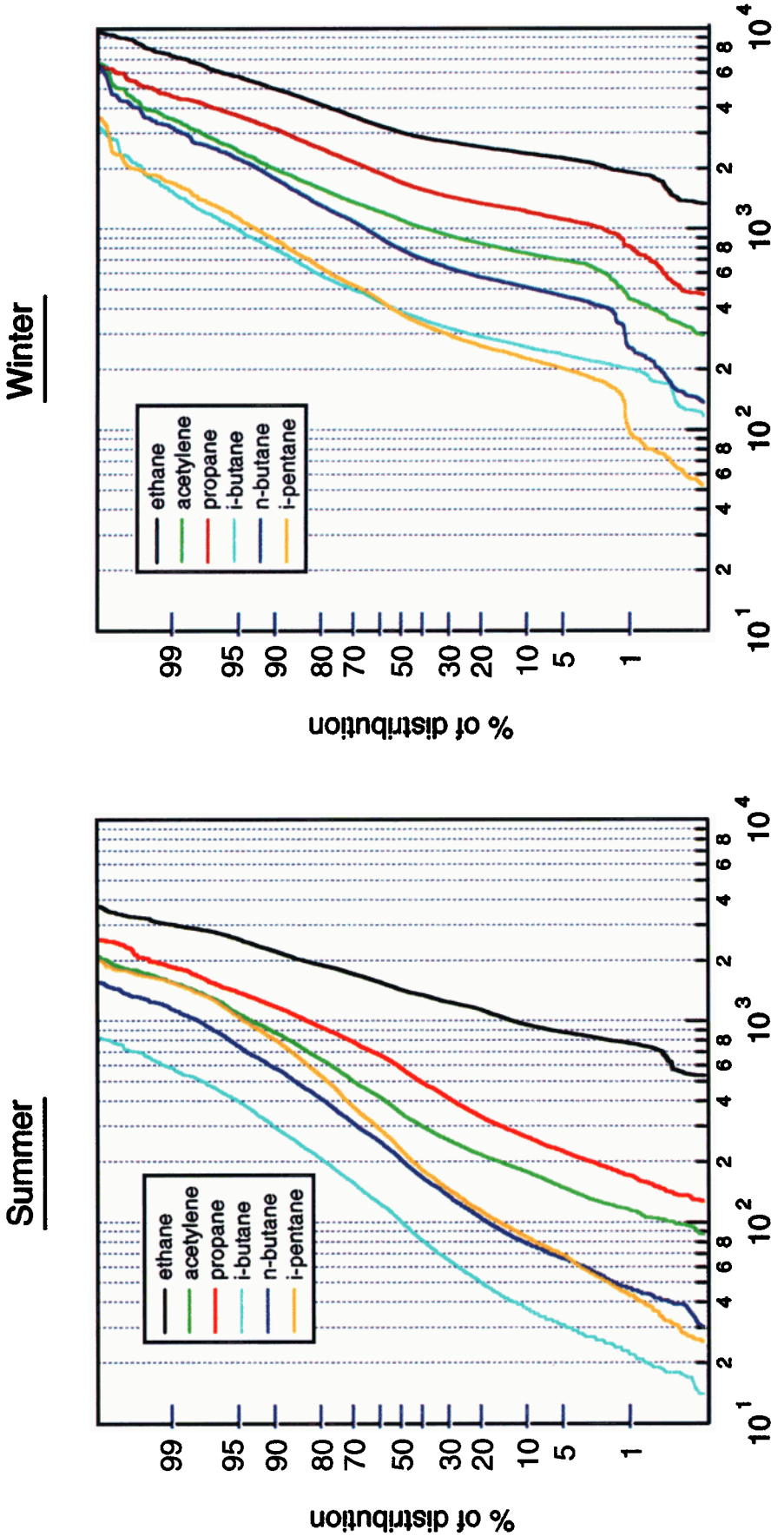


**Plate 2.** Cumulative distributions of selected hydrocarbon species measured at Harvard forest in summer (June, July, and August) and winter (December, January, and February) months.

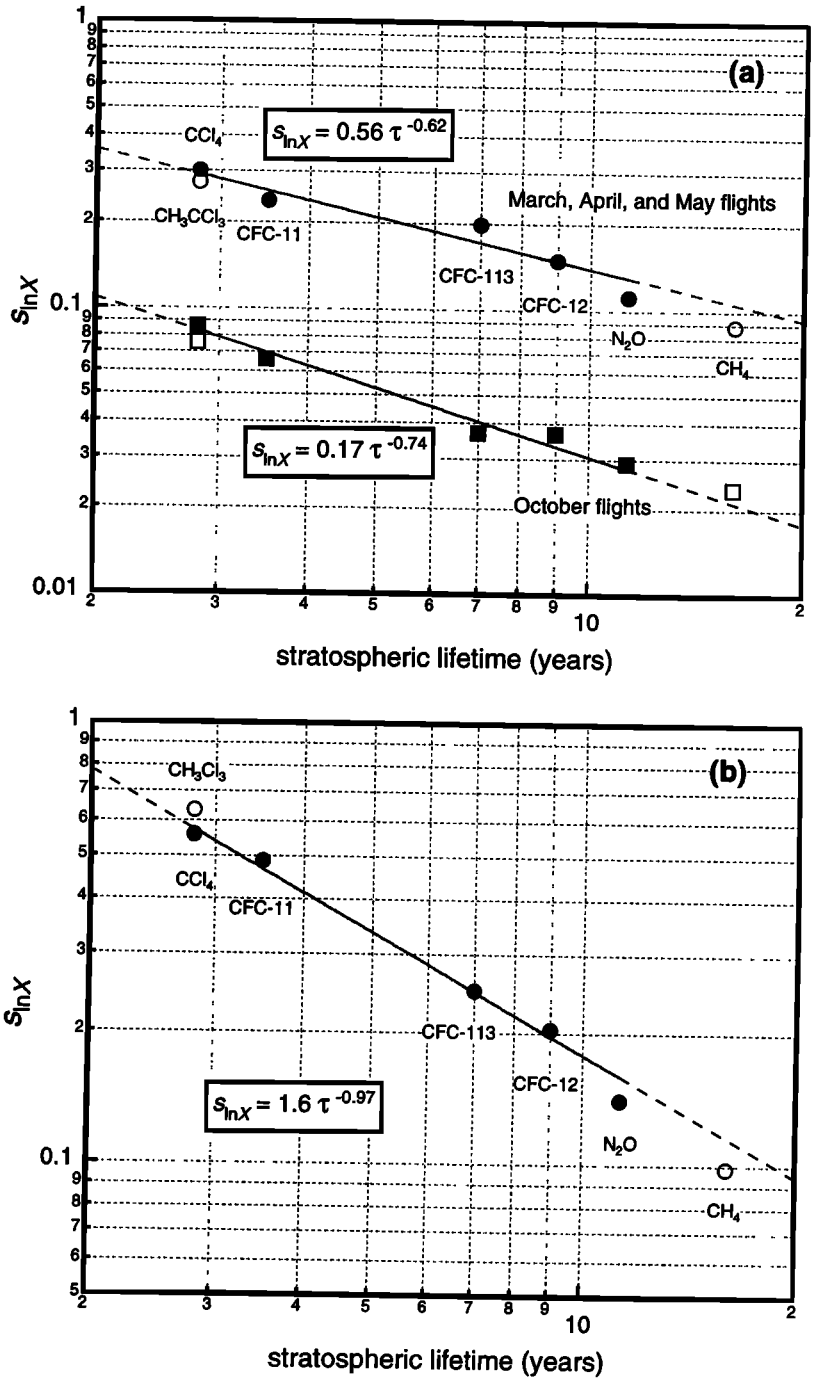


**Figure 7.** (a) The $s_{lnX}$ versus stratospheric lifetime for the ASHOE tropical flight data. Squares denote the October 24, 26, and 29 flight data. Circles denote the March 18, March 21, April 3, and May 20 flight data. Open symbols indicate that these data were not included in the regression fit. (b) The $s_{lnX}$ versus stratospheric lifetime for the ASHOE extratropical flight data.

driven by seasonal changes in removal rates. Mixing ratios are higher in winter than in summer, and in general, median mixing ratios increase with increasing lifetime. Two exceptions are noted: propane displays a higher mixing ratio than acetylene in both seasons even though propane has the shorter lifetime. This situation is likely a result of a larger regional emission strength for propane. The other exception is that *i*-pentane displays higher mixing ratios than the less reactive $C_4$ alkanes in summer. In winter, *i*-pentane and *i*-butane were observed at similar mixing ratios. This points to a significant seasonal change in the relative regional emission strengths of these compounds, either higher $C_4$ alkane emissions in winter or higher *i*-pentane emissions in summer or a combination of both. Figure 10 shows histograms of the ln of the hydrocarbon mixing ratios. Histograms of the summer data are reasonably symmetric about a median value. The winter data display more of a shoulder or tail at higher mixing ratios for all species. The mode and median of the winter data

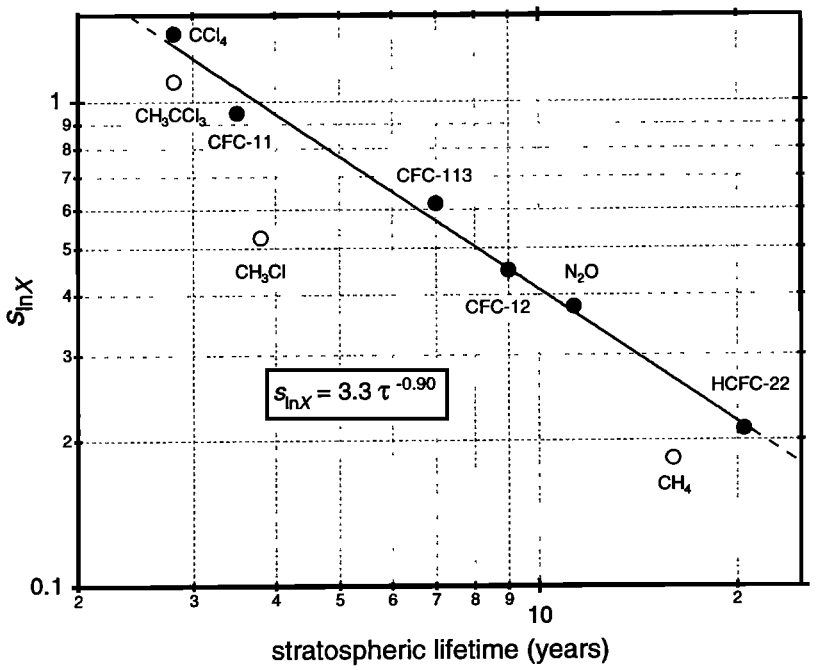


**Figure 8.** The $s_{lnX}$ versus stratospheric lifetime for the AASE II data. Open symbols indicate that these data were not included in the regression fit.

are clearly much larger than the summer median for all species but *i*-pentane.

In Figure 11a the winter to summer ratio of medians are plotted against HO rate coefficients. The seasonal change in the median mixing ratios (seasonal amplitude) shows a similar relationship to reactivity as that shown by *Goldstein et al.* [1995] for "background" mixing ratios, except that the amplitudes are smaller. Seasonal amplitudes for light alkanes typically increase with increasing hydrocarbon reactivity [*Jobson et al.*, 1994a, and references therein; *Penkett et al.*, 1993]. At Harvard forest there is a general increase in seasonal amplitude with reactivity for the $C_2$-$C_4$ hydrocarbons, but the $C_5$ alkanes and hexane fall well off this trend. Curiously, *i*-pentane displays less seasonal change than ethane, which could be a result of regional *i*-pentane emissions being higher in summer than winter. Changes in emission strengths obscure

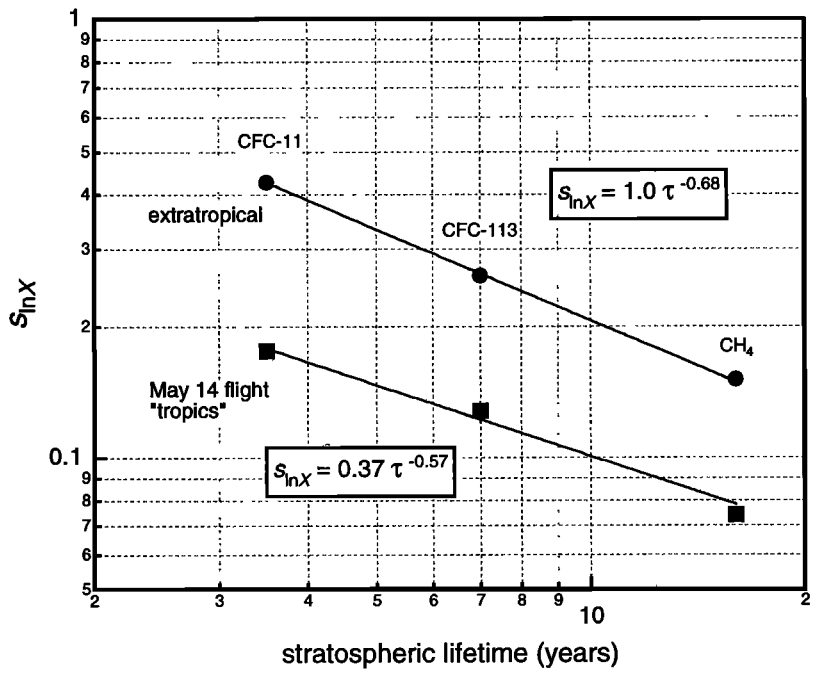


**Figure 9.** The $s_{lnX}$ versus stratospheric lifetime for the SPADE data. Extratropical data are shown as circles and tropical data as squares.

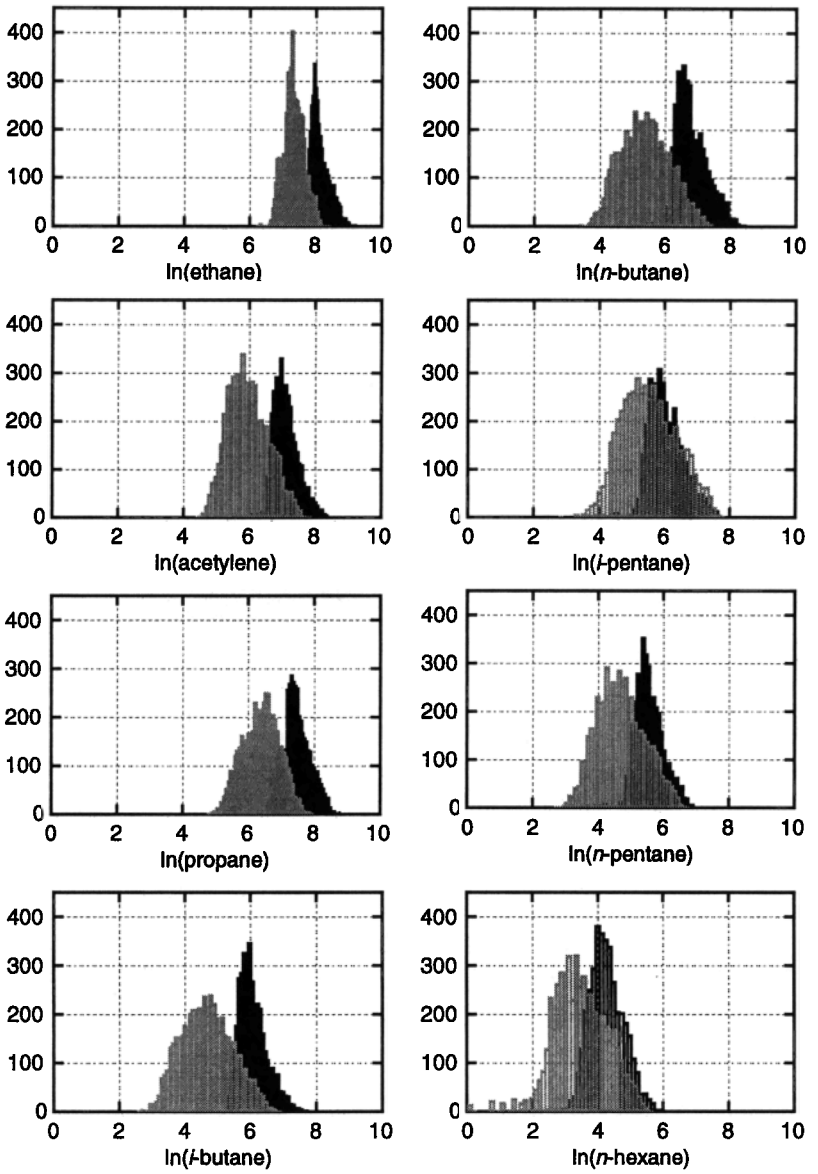


**Figure 10.** Histograms of ln of the mixing ratios for selected species measured during winter (black) and summer (shaded) months at Harvard forest. The y axis gives the number of samples within the mixing ratio interval range.

simple relationships between seasonal concentration changes and reactivity. In addition, mixing ratios of reactive species in summer will be more strongly influenced by local emission sources than longer-lived species. The small seasonal amplitudes for *i*-pentane, *n*-pentane, and hexane might reflect the greater influence of local sources on these species than on the longer-lived hydrocarbons.

The relationship between the summer to winter ratios of $s_{\ln X}$ and lifetime in Figure 11b shows different behavior. The more reactive a species, the greater its variability; therefore summer to winter ratios of $s_{\ln X}$ should be >1. With the exception of ethane and *i*-butane the $s_{\ln X}$ seasonal ratio was found to be surprisingly similar, averaging 1.54 ± 0.04. For ethane the $s_{\ln X}$ value was only 7% larger in summer, while for *i*-butane it was 74% larger. Ethane, however, displayed a distinctly different seasonal cycle of monthly $s_{\ln X}$ values than the other hydrocarbons. Monthly $s_{\ln X}$ values for ethane maximized in November (0.40) and minimized in April (0.15), and thus its cycle was ~3 months out of phase with the other hydrocarbons. Interestingly, using a 3 month averaging period over the minimum and maximum $s_{\ln X}$ periods for ethane yields a seasonal $s_{\ln X}$ amplitude of 1.57, similar to the other hydrocarbons. Figure 11c shows $s_{\ln X}$ versus lifetime for the summer and winter data. Lifetimes were calculated using the HO concentrations from *Goldstein et al.* [1995], which are a factor of 10 larger in summer than in winter, and the rate coefficients in Table 1. The summer and winter data appear to define a similar trend, except that the summer ethane data display a low variability. A fit through the winter data alone yields a $\tau^{-0.17 \pm 0.02}$ dependence. A fit through the summer data, excluding the ethane point, yields a similar $\tau^{-0.20 \pm 0.04}$ dependence, although the correlation is poorer. The choice of lifetimes does not influence the $\tau$ dependence, and thus there appears to be no significant seasonal change in the regional $\tau$

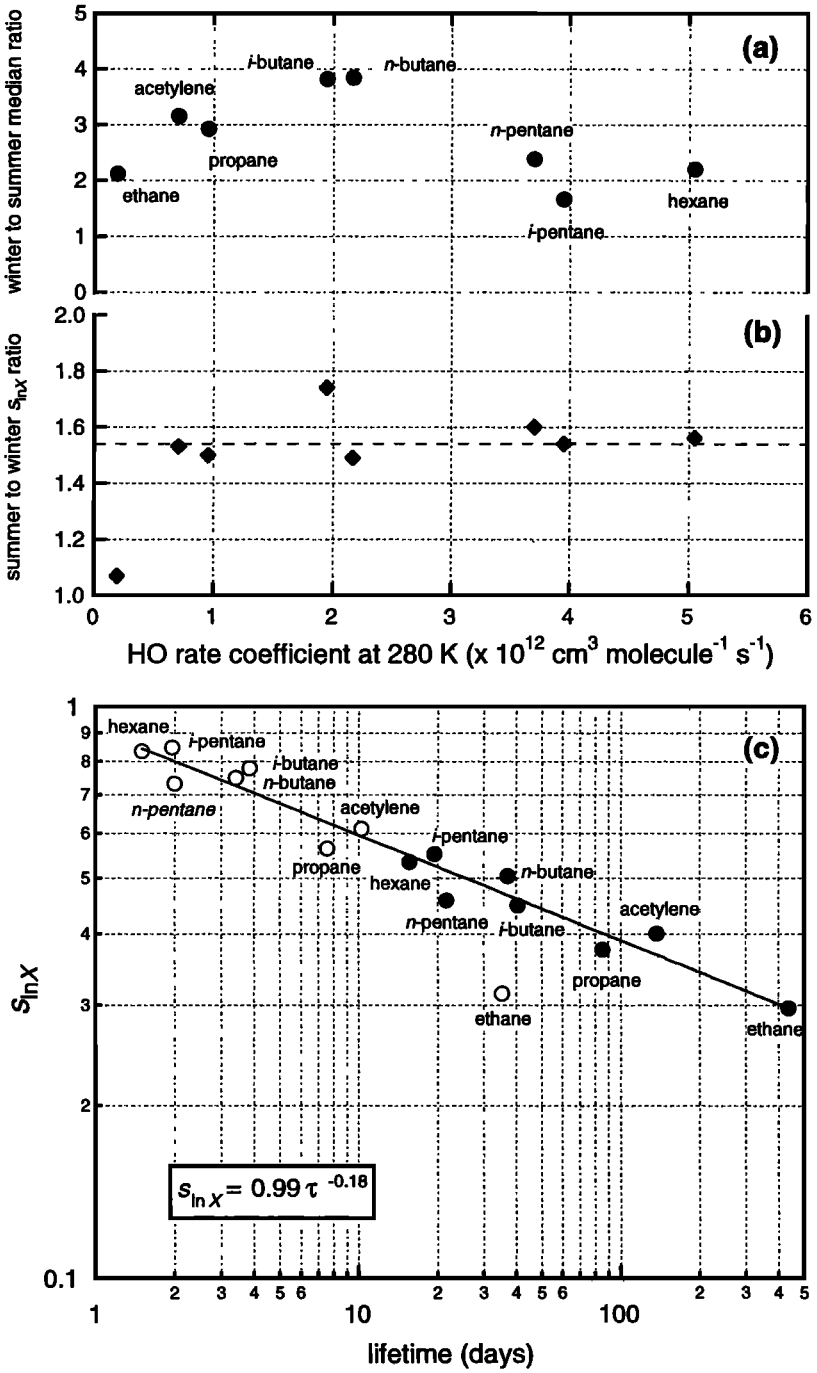


**Figure 11.** (a) The winter to summer ratio of median mixing ratios versus HO rate coefficients at 280 K. (b) The summer to winter ratio of $s_{lnX}$ versus HO rate coefficients at 280 K. The dashed line indicates an average value of 1.54. (c) A plot of $s_{lnX}$ versus lifetime for the summer data (open circles) and winter data (solid circles). The line is the fit through all the data excluding the summer ethane point.

dependence if the summer ethane data are excluded. Obviously, including ethane in a fit of the summer data would result in a significantly stronger $\tau$ dependence and an opposite conclusion to the one above. The data in Figure 11b offer a clue as to the correct interpretation. Excluding ethane, the data in Figure 11b display similar summer to winter ratios of $s_{lnX}$. This will occur if the winter and summer data have the same dependence on lifetime. Furthermore, an average $s_{lnX}$ ratio of 1.54 is consistent with a factor of 11 seasonal change in lifetime given the $\tau^{-0.18}$ dependence through the combined summer and winter data in Figure 11c.

It is not immediately clear why the ethane summer data are an outlier to the general trend. It may imply a difference in source geometry. For example, we argued that $CH_3Cl$ was below the trend in the PEM-West B data because of its broadly distributed source from the ocean. The 40 day ethane lifetime in summer gives it a much larger source footprint than the other species that have lifetimes <10 days. Far distant sources

can contribute a significant fraction of ethane mass to the site, and its source footprint is continental in scale. The short lifetimes of the other species qualitatively imply a regionalscale footprint. Therefore ethane variability may be influenced to a greater degree by nonregional sources, which result in a different variability-lifetime relationship than the other hydrocarbons. In winter the lifetimes of all species are >20 days, and it would appear that the species are influenced by the same source distribution. Interestingly, this larger source footprint in winter yields the same $\tau$ dependence as the summer footprint for reactive species.

*Moody et al.* [1998] have analyzed 48 hour back trajectories arriving at Harvard forest to assess the degree to which regional-scale transport influences trace gas concentrations measured at the site. Transport patterns were found to be similar between winter and summer. Highest hydrocarbon mixing ratios were associated with air parcels arriving from the southwest (a densely urbanized and industrialized area of the United States) and from more local origins. Lowest mixing ratios were associated with northern flow from Canada. They found that differences in regional wind flow explained a large amount of the hydrocarbon (specifically, acetylene and ethane) variability at the site. The weak $\tau$ dependence observed in the data is consistent with their conclusion.

### 2.4. Polar Sunrise Studies and Relative Radical Abundance

The depletion of $O_3$ within the marine boundary during polar sunrise has been observed at several Arctic locations [*Barrie et al.*, 1988; *Mickle et al.*, 1989; *Oltmans et al.*, 1989; *Solberg et al.*, 1996]. Associated with ozone-depleted air are low hydrocarbon mixing ratios. The changes in hydrocarbon mixing ratios and relative abundance compared to air above the marine boundary layer are highly correlated with the pattern expected for removal by Cl atoms [*Jobson et al.*, 1994b; *Solberg et al.*, 1996; *Ariya et al.*, 1998]. Alkylnitrate changes observed in ozone depleted air are also consistent with Cl atom chemistry [*Muthuramu et al.*, 1994]. In addition, very low mixing ratios of unsaturated species such as acetylene, trichloroethylene, and tetrachloroethylene imply the presence of Br atoms [*Jobson et al.*, 1994b; *Solberg et al.*, 1996; *Ariya et al.*, 1997, 1998], consistent with the hypothesis that the depleted ozone within the marine boundary layer is a result of Br atom attack [*Barrie et al.*, 1988]. Measurement sites located on the sea ice in the Lincoln Sea have observed extended periods (up to a week) where ozone mixing ratios are below detectable levels of ~1 ppbv [*Hopper et al.*, 1994, 1998]. Hydrocarbon canister samples collected at these sites also displayed very low mixing ratios [*Hopper et al.*, 1994; *Ariya et al.*, 1998].

The focus of this section is to examine the variability-lifetime relationship for the site described by Jobson et al. [1994b] and Hopper et al. [1994]. Because free tropospheric air is seldom sampled at these sea ice sites, it is difficult to analyze the hydrocarbon time series in terms of a contrast between free tropospheric air and halogen atom processed marine boundary layer air in order to extract a halogen chemistry signature. However, if we assume that there is a relationship between hydrocarbon variability and lifetime, then it is possible to extract the relative abundances of HO, Cl, and Br radicals. This possibility was suggested by *Jobson et al.* [1998] as a way of estimating HO concentrations relative to those of ozone; *Ehhalt et al.* [1998] have recently presented such an estimate.

Figure 12 shows the relationship between $s_{\ln X}$ and lifetime for the samples collected on the sea ice site in 1992. The hydrocarbon lifetimes are unknown because absolute radical concentrations are unknown but are assumed to be determined

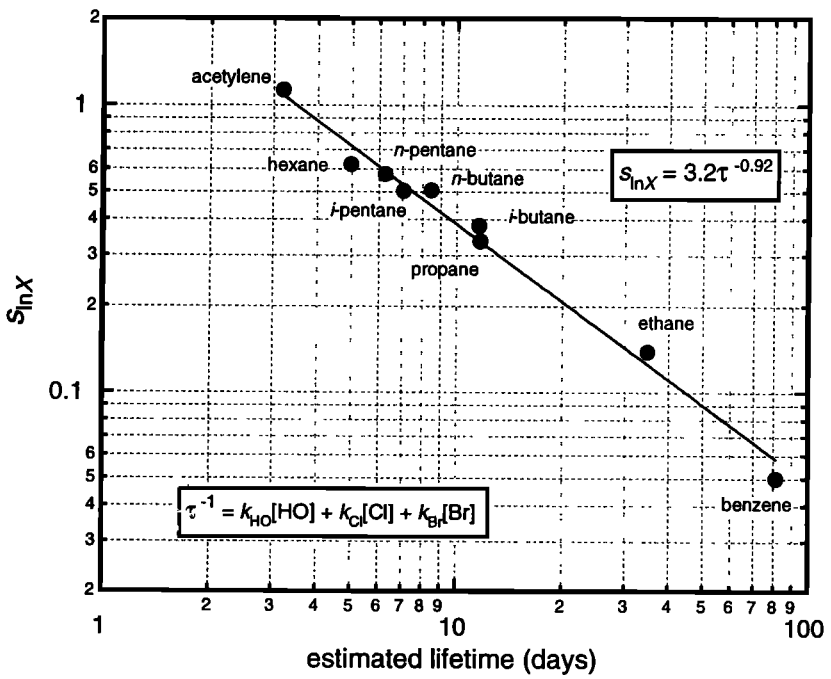


**Figure 12.** Polar Sunrise Experiment (PSE) 1992 data from a site on the sea ice north of Alert, Canada; plot is $s_{\ln X}$ versus estimated lifetime that includes contributions from Br and Cl atoms as well as HO. Best fit line is obtained with a relative HO:Cl:Br radical abundance of 17:1:3300.

by the oxidants HO, Cl, and Br. Local lifetimes are thus defined as

$$\tau = \frac{1}{k_{HO}[HO] + k_{Cl}[Cl] + k_{Br}[Br]} \quad (7)$$

Halogen atom rate coefficients were taken from *Hooshiyar and Niki* [1995] and *Atkinson and Aschmann* [1985]. Structure reactivity relationships [*Atkinson*, 1987] were used to calculate the HO + hydrocarbon rate coefficients for hexane and *i*-pentane. By assuming an arbitrary Cl atom concentration of 6 x $10^3$ atoms $cm^{-3}$ [*Ariya et al.*, 1998] and by appropriate adjustment of the relative amounts of HO and Br atom concentrations a highly correlated trend between $s_{\ln X}$ and lifetime develops. The best fit is given by a relative HO:Cl:Br radical abundance of ~17:1:3300. The resulting $\tau^{-0.92}$ dependence in the 1992 data is surprisingly strong and approaches the $b$=1 dependence expected for variability dominated by chemical loss [*Jobson et al.*, 1998]. This ratio of Br to Cl is higher than the 400-1200 range calculated from hydrocarbon trends at Alert during this time using a different approach [*Jobson et al.*, 1994b] but is similar to those calculated by *Ariya et al.* [1998] for the 1994 Polar Sunrise Experiment.

## 3. Discussion

### 3.1. The Exponent *b*

To this point we have demonstrated that coherent variability-lifetime relationships exist on the regional scale, both within the troposphere and the stratosphere over a wide range of lifetimes. The dependence on lifetime for the remote tropospheric data displays an approximate $\tau^{-0.5}$ dependence, much weaker than the *Junge* [1974] relationship and the stratospheric trends. The $\tau^{-0.5}$ dependence in remote areas is similar to that found by *Ehhalt et al.* [1998] in a 3-D CTM simulation of tracer relationships. The model results from *Ehhalt et al.* [1998] show a geographic distribution in the $\tau$ dependence, the farther away from sources, the larger the exponent $b$. The observations presented here follow the same general trend with the Harvard forest data displaying a weaker dependence than those found in the more remote NARE locations [*Jobson et al.*, 1998] and in the GTE data. Following Ehhalt's analysis, the exponent $b$ can be qualitatively viewed as an index that relates to source-receptor distances. The lower limit of $b$=0, which has been observed in urban data [*Jobson et al.*, 1998] and over source regions [*Ehhalt et al.*, 1998], indicates that the variability is driven by differences in the strengths of local sources that are in close proximity to the measurement location. The limit of $b$=1 was discussed in *Jobson et al.*, [1998] and can be considered the chemical kinetic limit where the variability is dominated by chemical loss alone. The Arctic data discussed in section 2.4 and the extratropical stratospheric data from ASHOE and AASE II approached this $b$=1 limit and suggest a remoteness or isolation from sources at these locations and therefore a variability that is driven largely by differences in the degree of photochemical processing of the sampled air masses. Interestingly the extratropical SPADE data displayed a significantly weaker $\tau$ dependence than the ASHOE or AASE II data. *Waugh et al.* [1997] noted that the tracer-tracer correlations for the SPADE mission were different than those of either the ASHOE or AASE II data and attributed this difference to the mixing of vortex air with midlatitude air. Evidence of this mixing was the appearance of a linear relationship between CFC-11 and $N_2O$ in a normally curved region of the correlation diagram. This mixing has evidently resulted in a weaker $\tau$ dependence in the SPADE data, though it should be noted that a much smaller latitude range was sampled in SPADE compared to ASHOE or AASE II. It has been our general working hypothesis that mixing amongst air parcels with different processing times would weaken the $\tau$ dependence. At this stage we have cradled the meaning of $b$ in terms of an index relating to source-receptor distances, although it may be more physically meaningful to view $b$ as an index that relates to mixing influences. Locations where widely different air mass ages are mixed will display smaller values of $b$. In the troposphere this will happen close to source regions where fresh emissions are dispersed into the more photochemically processed background air. The influence of mixing through concentration gradients gives rise to an overall distribution of $b$ that reflects distances from sources.

The stronger lifetime dependence, greater spatial variability, and generally lower mixing ratios in the extratropics compared to the tropical data are consistent with the notion of extratropical air being older and having passed through the higher altitude regions of the stratosphere where photochemical destruction of these gases occurs. The tropical air is more recently arrived to the stratosphere and, at the altitudes sampled by the ER2, has not had a chance to be thoroughly photochemically processed. The tropical region might be characterized as tropospheric air diluted with air that has been photochemically processed in the stratosphere, hence the weaker lifetime dependence but clear stratospheric processing signature.

### 3.2. The Coefficient *A*

In this paper we have focussed on the exponent $b$ and have not considered the physical meaning of the proportionality coefficient in (2). If it can be assumed that the measurements are an ensemble of air parcels with the same initial concentrations but varying transit times, then (2) can be rewritten as

$$s_{\ln X} = A\,\tau^{-b} = \left(\frac{\Psi}{\tau}\right)^{b} \quad (8)$$

where $\Psi$ is related to some measure of the transit time distribution from sources. For example, in the exponential model where $b$=1 [*Jobson et al.*, 1998], $\Psi$ is the standard deviation of the sampled transit times. The stratospheric data most closely follow (8) because concentrations of tracers entering the stratosphere are not thought to vary greatly except for species like HCFC-22, which have significant tropospheric growth rates. For tropospheric data this relationship is probably a poor approximation.

Equation (8) allows for an interesting comparison between model calculated transit time ranges in the stratosphere and those empirically determined from $s_{\ln X}$ versus $\tau$ relationships. For the extratropical data the values of $\Psi$ are 1.6 years for ASHOE and 3.8 years for AASE II; much larger than the ASHOE tropical values: 0.09 years for October and 0.39 years for March, April, and May. The lower tropical values are consistent with the range of calculated "age" estimates of stratospheric air where tropical air is not only young but displays little variation in age over a wide range of latitudes

[*Rosenlof*, 1995; *Hall and Waugh*, 1997]. This is in contrast to the extratropics where a wide range of ages can be encountered over a relatively small latitude range. For example, *Rosenlof* [1995] estimates Southern Hemisphere ages at 50 mbar ranging from ~3.5 to ~2 years, and a nearly uniform tropical age of ~0.75 years. Such stratospheric age estimates are considered to be averages of a probability density function of air parcel ages (or age spectrum) at a given altitude and latitude [*Rosenlof*, 1995; *Hall and Waugh*, 1997]. Again, it should be noted that the choice of lifetime definitions used in plotting the data does not affect the determination of the exponent $b$ but does influence $\Psi$. We have focused on evaluating $b$, but realizing that $\Psi$ may be physically meaningful for the stratosphere and therefore constrained by a physically plausible range of values imposes constraints on the estimated lifetimes. This may be useful for evaluating tracer lifetime estimates in the stratosphere. A more rigorous understanding of the physical meaning of the coefficients in (8) will require an examination of tracer relationships in a 3-D CTM.

### 3.3. The Meaning of $\ln(X_i)$ Versus $\ln(X_j)$ Correlations

As a final application of $s_{\ln X}$ analysis, we relate the relationships between $s_{\ln X}$ and lifetime to the more conventional analysis of $\ln(X_i)$ versus $\ln(X_j)$ tracer scatter plots between species $i$ and $j$. It has been noted within the troposphere that plots of ln(*n*-butane/ethane) versus ln(propane/ethane) yield very similar slopes (~1.40) or ~50% less than the kinetic slope (given by the ratio of the HO rate coefficient differences: $k_{n\text{-butane}}$-$k_{\text{ethane}}$ / $k_{\text{propane}}$-$k_{\text{ethane}}$). Such slopes have been observed for latitudinal gradients [*Rudolph and Johnen*, 1990], seasonal changes at background mid-latitude and high-latitude sites [*Jobson et al.*, 1994a, 1994b] and over a wide range of regional scales in the summertime [*Parrish et al.*, 1992]. Using the PEM-West A data set, *McKeen et al.* [1996] argue that this deviation from pure kinetics is a result of dilution with background air at a rate comparable to the lifetime of *n*-butane. Through the analysis of 3-D model tracer studies, *Ehhalt et al.* [1998] came to the same conclusion, and further illustrated how this deviation depends on the proximity of the sampling area to emission sources. *Ehhalt et al.* [1998] also suggested a power law relationship between the slopes of $\ln(X_i)$ versus $\ln(X_j)$ correlations and the ratio of species lifetimes. We show below that such a power law relationship follows naturally whenever $s_{\ln X}$ is related to $\tau$ as in Equation (2).

Analogous to the definition of standard deviation, for $n$ values of $X$;

$$S_{\ln X} = \sqrt{\frac{\sum_n (\ln X)^2 - \frac{1}{n}\left(\sum_n \ln X\right)^2}{n-1}} \tag{9}$$

A very useful relationship is derived from (9) if two species $X_i$ and $X_j$ are related by

$$\ln(X_i) = c + m \cdot \ln(X_j) \tag{10}$$

since substitution of (10) into (9), and eliminating common quadratic terms yields the simple relationship

$$S_{\ln X_i} = m \cdot S_{\ln X_j} \tag{11}$$

Equation (10) would only be expected to hold for species that have common sources and sinks. It should also be noted that using relative standard deviation (RSD) as a measure of variability [*Ehhalt et al.*, 1998] does not result in a simple relationship between the $m$ term in (10) and RSD. The $s_{\ln X}$ metric is therefore a more useful measure of variability for nonmethane hydrocarbons that can be accurately related by (11).

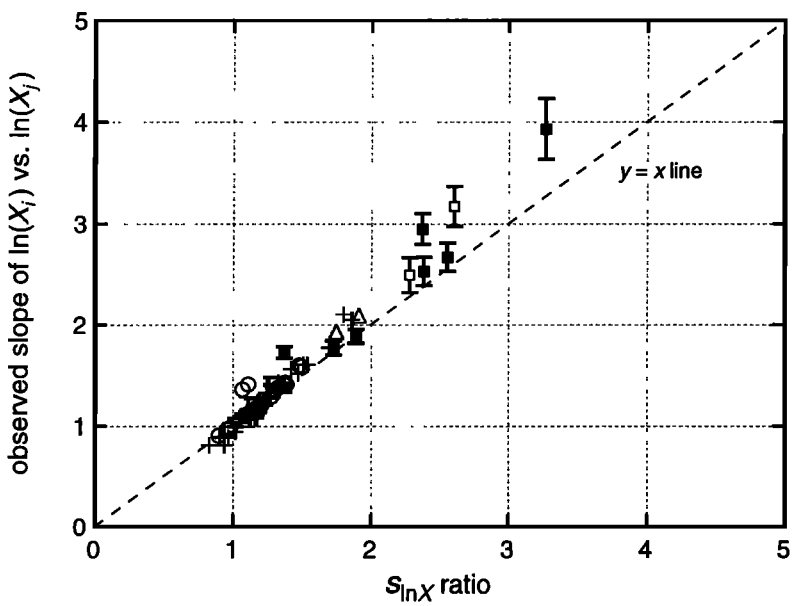


**Figure 13.** Plot of the observed slope of $\ln(X_i)$ versus $\ln(X_j)$ for tropospheric hydrocarbon data versus the ratio of their respective $s_{\ln X}$ values. One sigma error bars for the observed slopes are shown for the PEM-West B data (solid squares) and the ABLE 3B data (open squares). Other data shown are TRACE-A (triangles), Harvard forest winter data (crosses), and Harvard forest summer data (open circles).

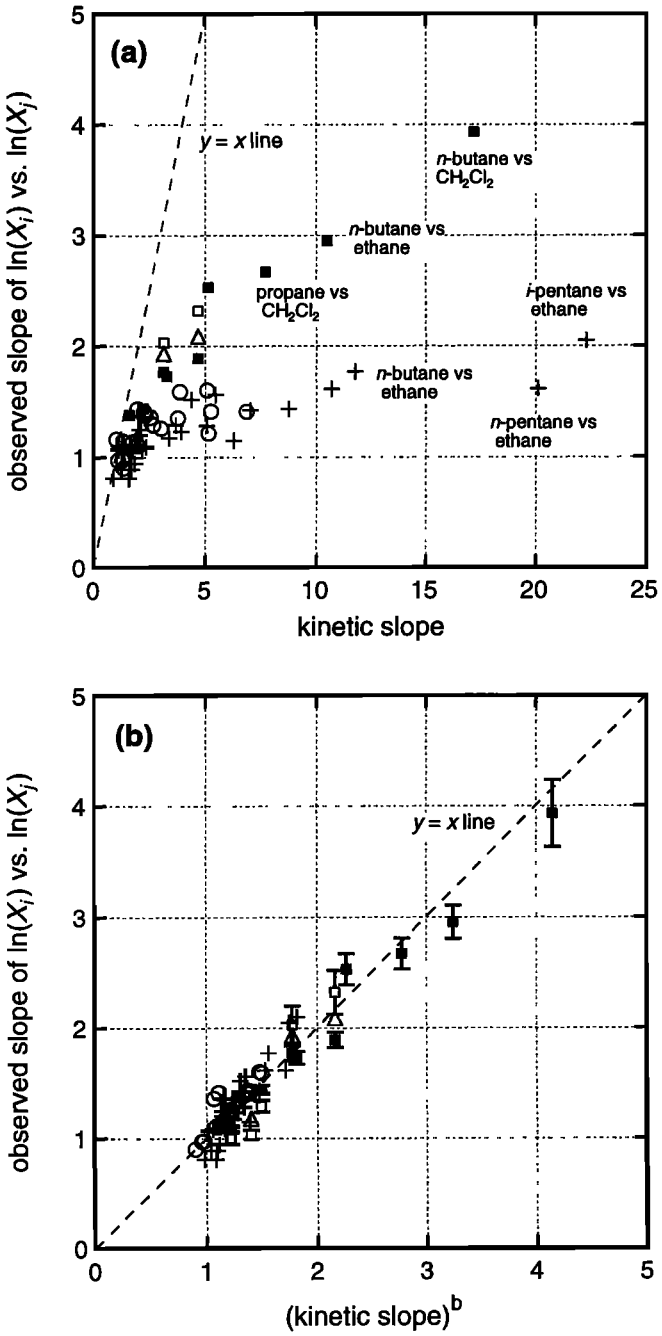


**Figure 14.** (a) Plot of the observed slope of $\ln(X_i)$ versus $\ln(X_j)$ for tropospheric hydrocarbon data versus the kinetic slope given by the ratio of the species lifetimes ($\tau_j/\tau_i$). (b) Plot of the observed slope of $\ln(X_i)$ versus $\ln(X_j)$ versus the appropriately power-transformed kinetic slope. PEM-West B data (solid squares, $b$=0.5), ABLE 3B data (open squares, $b$=0.5), TRACE-A (triangles, $b$=0.5), Harvard forest winter data (crosses, $b$=0.18), and Harvard forest summer data (open circles, $b$=0.18).

Figure 13 tests the relationship between (10) and (11) by comparing variability ratios and the slope of $\ln(X_i)$ versus $\ln(X_j)$ correlations from the various tropospheric data sets incorporated in this study. Shown are only those data from scatter plots where the correlation coefficient $r > 0.8$. The slopes through the data were determined by a linear regression that assumed uncertainty in both variables. Some field campaigns exhibited poor correlations between species although yielded an overall coherent $s_{\ln X}$ versus lifetime trend (i.e., TRACE-A). Figure 13 shows that (11) relates the variability in the observations to the slopes of ln correlation plots remarkably well, especially for those species that have variability ratios <2. Those correlations that do not adhere to (11) are species with large differences in photochemical lifetimes (i.e., hexane and ethane), which generally display lower correlations, as discussed above.

By combining (2) and (11), one derives the relationship between $m$ and $\tau$:

$$m = \left(\frac{\tau_j}{\tau_i}\right)^b \tag{12}$$

where $b$ is determined from the slope of $s_{\ln X}$ versus $\tau$ correlations (e.g., (2)). Equation (12) is very similar to that proposed by *Ehhalt et al.* [1998, equation (22)], and the $b$ term in (12) is equivalent to the $a_{ij}$ term within their paper. The difference between the two approaches is that the $b$ term is a constant, independent of the value of $\tau_i$ and $\tau_j$, whereas their $a_{ij}$ is a variable that depends on the particular species pair plotted. This difference is a consequence of using RSD as a measure of variability. For very skewed statistical distributions the RSD statistic tends to asymptotically approach a constant value for short lived species [cf. *Jaenicke*, 1982; *Slinn*, 1988].

In Figure 14a the observed slope of $\ln(X_i)$ versus $\ln(X_j)$ scatter plots is shown as a function of the kinetic slope (given by the ratio of the lifetimes: $\tau_j/\tau_i$). Clearly the observed slopes are not linear functions of the kinetic slope and fall well off the $y$=$x$ line when species lifetimes become significantly different. The largest difference between observed and kinetic slopes are for the Harvard forest winter data. Figure 14b tests the relationship in (12). The linear relationship between the observed slope and the power transformed kinetic slope (given by $(\tau_j/\tau_i)^b$) fall about the $y$=$x$ line. Returning to the nature of the ln($n$-butane/ethane) versus ln(propane/ethane) slopes, we conclude that the similarity in slopes from different locations results from the similarity in the regional $s_{\ln X}$ versus lifetime dependence. Knowing the power law relationship allows a straightforward analytical interpretation of the observed slopes of $\ln(X_i)$ versus $\ln(X_j)$ plots that is independent of assumptions about the regional background. This highlights an important point as correlation plots are a key tool for organizing data and relating relative changes in concentration to photochemical processes. In particular, within the troposphere the study of the photochemical transformation of constituents such as $NO_x$, NOy, CO and $O_3$ in urban and power plant plumes often relies on the use of correlations between these species as a means of understanding the underlying photochemistry and their relative rates of production and loss.

## 4. Summary and Conclusion

In this paper we have examined previously published data sets of hydrocarbons, halocarbons, and CFCs to investigate the relationship between variability and lifetime on a regional scale. The data examined were collected in the troposphere and stratosphere. The standard deviation of the ln-transformed data ($s_{\ln X}$) was used as a comparative measure of trace gas variability. Variability was found to follow a power law relationship with lifetime given by (2). The lifetime dependence given by the exponent $b$ differed considerably

between the data sets and relates the relative importance of sources and sinks in describing regional variability of trace gases. In the GTE data sets the correlation between $s_{\ln X}$ and lifetime spanned a lifetime range of 4 orders of magnitude. The dependence on lifetime for these remote tropospheric data was $\sim\tau^{-0.50}$, with the proportionality factor $A$ varying between the different field campaigns. Some species, such as $CH_3Cl$ and the halons, did not fall along the trends. The low variability of $CH_3Cl$ relative to the trend may illustrate the importance of its oceanic source in determining its spatial variability.

The Harvard forest hydrocarbon data displayed no seasonal dependence in the variability-lifetime relationship. The summer to winter $s_{\ln X}$ ratios may therefore provide a means of estimating the relative change in HO concentrations on a regional scale. The average ratio of summer to winter $s_{\ln X}$ values of 1.54 is consistent with the *Goldstein et al.* [1995] estimated factor of 10 seasonal change in lifetime given the observed $\tau^{-0.18}$ dependence.

The stratospheric data displayed a strongly correlated trend between $s_{\ln X}$ and stratospheric lifetime. There is still much uncertainty regarding stratospheric lifetimes. On the basis of the good correlation obtained we used the CTM-derived lifetimes from *Avallone and Prather* [1997]. Both the ASHOE and AASE II extratropical data displayed a very strong lifetime dependence, $\tau^{-0.97}$ and $\tau^{-0.90}$, respectively, much stronger than the tropospheric data. Tropical data from the stratosphere generally displayed a significantly weaker $\tau$ dependence than the extratropical data. The proportionality coefficient $\Psi$ was also much smaller for the tropical data. The value of $\Psi$ compared well to published estimates of chronological age ranges of stratospheric air for the tropical and extratropical regions sampled by the ER2 and supports the idea that $\Psi$ is likely some measure of the source-receptor transit time range implicit in the tracer measurements.

We also examined a small data set collected on the sea ice of the Lincoln Sea during the spring of 1992 where hydrocarbon distributions suggest the occurrence of Cl and Br atom oxidation in the Arctic. The time series data were used to illustrate the point that regional variability-lifetime relationships for hydrocarbons might be profitably used to estimate the relative abundance of radicals. The approach assumes that such a relationship exists (but makes no assumptions regarding the lifetime dependence) and that the relevant rate coefficients are well known. The estimated Br:Cl ratio found from the variability-lifetime approach was similar to those estimated at Alert during the same period using a different approach.

Finally, we have shown how the variability-lifetime relationships can help in the interpretation of ln versus ln correlation plots of tracers such as ln[$n$-butane] versus ln[propane] commonly considered in the troposphere. Plots of $\ln(X_i)$ versus $\ln(X_j)$ are often highly correlated linear trends for which a slope can be determined with confidence, particularly in the stratosphere. The coefficient $b$ in (2) gives the appropriate power transformation in order to relate linearly the observed slope of $\ln(X_i)$ versus $\ln(X_j)$ plots to their kinetic slope. Equation (2) promises to be a powerful analytical tool for understanding the relative influence of sources and sinks on the variability of reactive trace gases and for understanding the relationships amongst these gases in the atmosphere.

**Acknowledgments.** We would like to thank K. Rosenlof, A. Tuck, and S. Solomon for helpful discussions and pointers.

## References


Anderson, J.G., and O.B. Toon, Airborne Arctic Stratospheric Expedition II: An overview, *Geophys. Res. Lett.*, *20*, 2499-2502, 1993.

Ariya, P.A., B.T. Jobson, R. Sander, H. Niki, G.W. Harris, J.F. Hopper, and K.G. Anlauf, Measurements of $C_2$-$C_7$ hydrocarbons during the Polar Sunrise Experiment 1994: Further evidence for halogen chemistry in the troposphere, *J. Geophys. Res.*, *103*, 13,169-13,180, 1998.

Ariya, P.A., V. Catoire, R. Sander, H. Niki, and G.W. Harris, Trichloroethene and tetrachloroethene: Tropospheric probes for Cl- and Br-atom reactions during polar sunrise, *Tellus*, *49B*, 583-591, 1997.

Atkinson, R., A structure-activity relationship for the estimation of rate constants for the gas-phase reactions of OH radicals with organic compounds, *Int. J. Chem. Kinet.*, *19*, 799-828, 1987.

Atkinson, R., Kinetics and mechanisms of the gas-phase reactions of the hydroxyl radical with organic compounds, *J. Phys. Chem. Ref. Data Monogr. 1*, 121-126, 1989.

Atkinson, R., Gas-phase tropospheric chemistry of organic compounds, *J. Phys. Chem. Ref. Data Monogr. 2*, 75-116, 1994.

Atkinson, R.A., and S.M. Aschmann, Kinetics of the gas phase reaction of Cl atoms with a series of organics at 296 ± 2K and atmospheric pressure, *Int. J. Chem. Kinet.*, *17*, 33-41, 1985.

Avallone, L.M., and M.J. Prather, Tracer-tracer correlations: Three-dimensional model simulations and comparisons to observations, *J. Geophys. Res.*, *102*, 19,233-19,246, 1997.

Barrie, L.A., J.W. Bottenheim, R.C. Schnell, P.J. Crutzen, and R.A. Rasmussen, Ozone destruction and photochemical reactions at polar sunrise in the lower Arctic atmosphere, *Nature*, *334*, 138-141, 1988.

Blake, D.R., and F.S. Rowland, Global atmospheric concentrations and source strength of ethane, *Nature*, *321*, 231-233, 1986.

Blake, D.R., T.W. Smith, T.-Y. Chen, W.J. Whipple, and F.S. Rowland, Effects of biomass burning on summertime nonmethane hydrocarbon concentrations in the Canadian wetlands, *J. Geophys. Res.*, *99*, 1699-1719, 1994.

Blake, N.J., D.R. Blake, B.C. Sive, T.-Y. Chen, F.S. Rowland, J.E. collins, G.W. Sachse, and B.E. Anderson, Biomass burning emissions and vertical distribution of methyl halides and other reduced carbon gases in the South Atlantic region, *J. Geophys. Res.*, *101*, 24,151-24,164, 1996.

Blake, N.J., D.R. Blake, T.-Y. Chen, J.E. Collins, G.W. Sachse, B.E. Anderson and F.S. Rowland, Distribution and seasonality of selected hydrocarbons and halocarbons over the western Pacific basin during PEM West A and PEM West B, *J. Geophys. Res.*, *102*, 28,315-28,331, 1997.

Ehhalt, D.H., F. Rohrer, A. Wahner, M.J. Prather, and D.R. Blake, On the use of hydrocarbons for the determination of tropospheric OH concentrations, *J. Geophys. Res.*, *103*, 18,981-18,997, 1998.

Elkins, J.W., et al., Airborne gas chromatograph for in situ measurements of long-lived species in the upper troposphere and lower stratosphere, *Geophys. Res. Lett.*, *23*, 347-350, 1996.

Fishman, J., J.M. Hoell, R.D. Bendura, R.J. McNeal, and V.W.J.H. Kirchhoff, NASA GTE TRACE A experiment, *J. Geophys. Res.*, *101*, 23,865-23,880, 1996.

Goldstein, A.H., S.C. Wofsy, and C.M. Spivakovsky, Seasonal variations of nonmethane hydrocarbons in rural New England: Constraints on OH concentrations in northern midlatitudes, *J. Geophys. Res.*, *100*, 21,023-21,033, 1995.

Gregory, G.L., H.E. Fuelberg, S.P. Longmore, B.E. Anderson, J.E. Collins, and D.R. Blake, Chemical characteristics of tropospheric air over the tropical South Atlantic Ocean: Relationship to trajectory history, *J. Geophys. Res.*, *101*, 23,957-23,972, 1996.

Gregory, G.L., J.T. Merrill, M.C. Shipman, D.R. Blake, G.W. Sachse, and H.B. Singh, Chemical characteristics of tropospheric air over the Pacific Ocean as measured during PEM-West B: Relationship to Asian outflow and trajectory history, *J. Geophys. Res.*, *102*, 28,275-28,285, 1997.

Hall, T.M., and D.W. Waugh., Timescales for the stratospheric circulation derived from tracers, *J. Geophys. Res.*, *102*, 8991-9001, 1997.

Hamrud, M., Residence time and spatial variability for gases in the atmosphere, *Tellus*, *35 Ser. B*, 295-303, 1983.

Harriss, R.C., S.C. Wofsy, J.M. Hoell, R.J. Bendura, J.W. Drewry, R.J. McNeal, D. Pierce, V. Rabine, and R.L. Snell, The Arctic Boundary Layer Expedition (ABLE-3B): July-August 1990, *J. Geophys. Res.*, *99*, 1635-1643, 1994.

Hoell, J.M, D.D. Davis, S.C. Liu, R.E. Newell, H. Akimoto, R.J. McNeal, and R.J. Bendura, The Pacific Exploratory Mission-West Phase B: February-March, 1994, *J. Geophys. Res.*, *102*, 28,223-28,239, 1997.

Hooshiyar, P.A., and H. Niki, Rate constants for the gas-phase reactions of Cl-atoms with $C_2$-$C_8$ alkanes at $T$=296 ±2K, *Int. J. Chem. Kinet.*, *27*, 1197-1206, 1995.

Hopper, J.F., B. Peters, Y. Yokouchi, H. Niki, B.T. Jobson, P.B. Shepson, and K. Muthuramu, Chemical and meteorological observations at ice camp SWAN during Polar Sunrise Experiment 1992, *J. Geophys. Res., 99*, 25,489-25,498, 1994.

Hopper, J.F., L.A. Barrie, A. Silis, W. Hart, A.J. Gallant, and H. Dryfhout, Ozone and meteorology during the 1994 Polar Sunrise Experiment, *J. Geophys. Res., 103*, 1481-1492, 1998.

Jaenicke, R., Physical aspects of the atmospheric aerosol, in *Chemistry of the Polluted and Unpolluted Troposphere*, edited by H.W. Georgi and W. Jaeschke, D. Reidel, Norwell Mass., 1982.

Jobson, B.T., Z. Wu, H. Niki, and L. Barrie, Seasonal trends of isoprene, $C_2$-$C_5$ alkanes, and acetylene at a remote boreal site in Canada, *J. Geophys. Res., 99*, 1589-1599, 1994a.

Jobson, B.T., H. Niki, Y. Yokouchi, J. Bottenheim, F. Hopper, and R. Leaitch, Measurements of $C_2$-$C_6$ hydrocarbons during the Polar Sunrise 1992 Experiment: Evidence for Cl atom and Br atom chemistry, *J. Geophys. Res., 99*, 25,355-25,368, 1994b.

Jobson, B.T., D.D. Parrish, P. Goldan, W. Kuster, F.C. Fehsenfeld, D.R. Blake, N.J. Blake, and H. Niki, Spatial and temporal variability of nonmethane hydrocarbon mixing ratios and their relation to photochemical lifetime, *J. Geophys. Res., 103*, 13,557-13,567, 1998.

Junge, C.E., Residence time and variability of tropospheric trace gases, *Tellus, 26*, 477-488, 1974.

Kaye, J.A., S.A. Penkett, and F.M. Ormond editors., Report on concentrations, lifetimes, and trends of CFCs, halons and related species, *NASA Ref. Publ. 1339*, 2-1 to 2-26, 1994.

Klemp, D., D. Kley, F. Kramp, H.J. Buers, G. Pilwat, F. Flocke, H.W. Patz, and A. Volz-Thomas, Long-term measurements of light hydrocarbons ($C_2$-$C_5$) at Schauinsland (Black Forest), *J. Atmos. Chem., 28*, 135-171, 1997.

McKeen, S.A., S.C. Liu, E.-Y. Hsie, X. Lin, J.D. Bradshaw, S. Smyth, G.L. Gregory, and D.R. Blake, Hydrocarbon ratios during PEM-West A: A model perspective, *J. Geophys. Res., 101*, 2087-2109, 1996.

Mickle, R.E., J.W. Bottenhiem, W.R. Leaitch, and W. Evans, Boundary-layer ozone depletion during AGASP-II, *Atmos. Environ., 23*, 2443-2449, 1989.

Moody, J.L., J.W. Munger, A.H. Goldstein, D.J. Jacob, and S.C. Wofsy, Harvard Forest regional-scale air mass composition by patterns in atmospheric transport history (PATH), *J. Geophys. Res., 103*, 13,181-13,194, 1998.

Muthuramu, K., P.B. Shepson, J.W. Bottenheim, B.T. Jobson, H. Niki, and K.G. Anlauf, Relationships between organic nitrates and surface ozone destruction during the Polar Sunrise Experiment 1992, *J. Geophys. Res., 99*, 25,360-25,378, 1994.

Oltmans, S.J., L.A. Barrie, E.A. Atlas, L.E. Heidt, H. Niki, R.A. Rasmussen, and P.B. Shepson, Seasonal surface ozone and filterable bromine relationships in the high Arctic, *Atmos. Environ., 23*, 2431-2441, 1989.

Parrish, D.D., C.J. Hahn, E.J. Williams, R.B. Norton, F.C. Fehsenfeld, H.B. Singh, J.D. Shetter, B.W. Gandrud, and B.A. Ridley, Indications of photochemical histories of Pacific air masses from measurements of atmospheric trace species at Pt. Arena, California, *J. Geophys. Res., 97*, 15,883-15,902, 1992.

Penkett, S.A., N.J. Blake, P. Lightman, A.W.R Marsh, P. Anwyl, and G. Butcher, The seasonal variation of nonmethane hydrocarbons in the free troposphere over the North Atlantic Ocean: Possible evidence for the extensive reaction of hydrocarbons with the nitrate radical, *J. Geophys. Res., 98*, 2865-2885, 1993.

Prather, M., and C.M. Spivakovsky, Tropospheric OH and the lifetimes of hydrochlorofluorocarbons, *J. Geophys. Res., 95*, 18,723-18,729, 1990.

Prinn, R.G., R.F. Weiss, B.R. Miller, J. Huang, F.N. Alyea, D.M. Cunnold, P.J. Fraser, D.E. Hartley, and P.G. Simmonds, Atmospheric trends and lifetime of $CH_3CCl_3$ and global OH concentrations, *Science, 269*, 187-192, 1995.

Rosenlof, F.H., Seasonal cycle of the residual mean circulation in the stratosphere, *J. Geophys. Res., 100*, 5173-5191, 1995.

Rudolph, J., and F.J. Johnen, Measurements of light atmospheric hydrocarbons over the Atlantic in regions of low biological activity, *J. Geophys. Res., 95*, 20,583-20,591, 1990.

Rudolph, J., A. Khedim, R. Koppmann, and B. Bonsang, Field study of the emissions of methyl chloride and other halocarbons from biomass burning in western Africa, *J. Atmos. Chem., 22*, 67-80, 1995.

Singh, H.B., and L.J. Salas, Measurements of selected light hydrocarbons over the Pacific Ocean: Latitudinal and seasonal variations, *Geophys. Res. Lett., 9*, 842-845, 1982.

Singh, H.B., L.J. Salas, and R.E. Stiles, Methyl halides in and over the eastern pacific (40°N-32°S), *J. Geophys. Res., 88*, 3684-3690, 1983.

Slinn, W.G.N, A simple model for Junge's relationship between concentration fluctuations and residence times for tropospheric trace gases, *Tellus, Ser. B, 40*, 229-232, 1988.

Solberg, S., N. Schmidbauer, A. Semb, and F. Strodal, Boundary-layer ozone depletion as seen in the Norwegian Arctic spring, *J. Atmos. Chem., 23*, 301-332, 1996.

Spivakovsky, C.M., R. Yevich, J.A. Logan, S.C. Wofsy, and M.B. McElroy, Tropospheric HO in a three-dimensional chemical tracer model: An assessment based on observations of $CH_3CCl_3$, *J. Geophys. Res., 95*, 18,441-18,471, 1990.

Talbot, R.W., et al., Chemical characteristics of continental outflow over the tropical South Atlantic Ocean from Brazil and Africa, *J. Geophys. Res., 101*, 24,187-24,202, 1996.

Talbot, R.W., et al., Chemical characteristics of continental outflow from Asia to the troposphere over the western Pacific Ocean during February-March 1994: Results from PEM-West B, *J. Geophys. Res., 102*, 28,255-28,274, 1997.

Talukdar, R.K., A. Mellouki, T. Gierczak, S. Barone, S-Y. Chiang, and A.R. Ravishankara, Kinetics of the reactions of OH with alkanes, *Int. J. Chem. Kinet.*, 26, 973-990, 1994.

Tuck, A.F., W.H. Brune, and R.S. Hipskind, Airborne Southern Hemisphere ozone experiment/measurements for assessing the effects of stratospheric aircraft (ASHOE/MAESA): A road map, *J. Geophys. Res., 102*, 3901-3904, 1997.

Volk, C.M., J.W. Elkins, D.W. Fahey, G.S. Dutton, J.M. Gilligan, M. Loewenstein, J.R. Podolske, K.R. Chan, and M.R. Gunson, Evaluation of source gas lifetimes from stratospheric observations, *J. Geophys. Res., 102*, 25,543-25,564, 1997.

Waugh, D.W., et al., Mixing of polar vortex air into middle latitudes as revealed by tracer-tracer scatter plots, *J. Geophys. Res., 102*, 13,119-13,134, 1997.

Wofsy, S.C., S.-M. Fan, D.R. Blake, J.D. Bradshaw, S.T. Sandholm, H.B. Singh, G.W. Sachse, and R. C. Harris, Factors influencing atmospheric composition over the subarctic North America during summer, *J. Geophys. Res., 99*, 1887-1897, 1994a.

Wofsy, S.C., R.C. Cohen, and A.L. Schmeletopf, Overview: The stratospheric Photochemistry aerosols and dynamics expedition (SPADE) and airborne arctic stratosphere expedition II (AASE-II), *Geophys. Res. Lett., 21*, 2535-2538, 1994b.

Woodbridge, E.L., et al., Estimates of total organic and inorganic chlorine in the lower stratosphere from in situ and flask measurements during AASE II, *J. Geophys. Res., 100*, 3057-3064, 1995.

World Meteorological Organization (WMO), Scientific assessment of ozone depletion:1994, Global Ozone Res. and Monit. Proj., Rep. 37, Geneva, 1995.

Young, V.L., B.N Kieser, S.P. Chen, and H. Niki, Seasonal trends and local influences on nonmethane hydrocarbon concentrations in the Canadian boreal forest, *J. Geophys. Res., 102*, 5913-5918, 1997.

D.R. Blake, Department of Chemistry, University of California, Irvine, CA, 92717-2025.

J.W. Elkins, NOAA Climate Monitoring and Diagnostics Laboratory, 325 Broadway, Boulder, CO 80303.

F.C. Fehsenfeld and D.D. Parrish, NOAA Aeronomy Laboratory, 325 Broadway, Boulder, CO 80303.

A.H. Goldstein, ESPM Ecosystems Sciences Division, University of California, Berkeley, CA 94720-3110.

B.T. Jobson and S.A. McKeen, Cooperative Institute for Research in Environmental Science, University of Colorado, Boulder, CO 80303. (tjobson@al.noaa.gov).

S.M. Schauffler, National Center for Atmospheric Research, 1850 Table Mesa Drive, Boulder, CO 80307.

(Received October 29, 1998; revised January 28, 1999;
accepted February 19, 1999.)